Article

Sex-specific adipose tissue imprinting of regulatory T cells

https://doi.org/10.1038/s41586-020-2040-3

Received: 24 October 2018

Accepted: 14 January 2020

Published online: 26 February 2020

Check for updates

Ajithkumar Vasanthakumar[1,2]✉, David Chisanga[2,3], Jonas Blume[1,2], Renee Gloury[1,2], Kara Britt[4], Darren C. Henstridge[5], Yifan Zhan[2,3], Santiago Valle Torres[1], Sebastian Liene[1,6], Nicholas Collins[1], Enyuan Cao[7], Tom Sidwell[1,2], Chaoran Li[8], Raul German Spallanzani[8], Yang Liao[2,3], Paul A. Beavis[4], Thomas Gebhardt[1], Natalie Trevaskis[7], Stephen L. Nutt[2,3], Jeffrey D. Zajac[9], Rachel A. Davey[9], Mark A. Febbraio[7], Diane Mathis[8], Wei Shi[2,10] & Axel Kallies[1,2]✉

Adipose tissue is an energy store and a dynamic endocrine organ[1,2]. In particular, visceral adipose tissue (VAT) is critical for the regulation of systemic metabolism[3,4]. Impaired VAT function—for example, in obesity—is associated with insulin resistance and type 2 diabetes[5,6]. Regulatory T (T_{reg}) cells that express the transcription factor FOXP3 are critical for limiting immune responses and suppressing tissue inflammation, including in the VAT[7–9]. Here we uncover pronounced sexual dimorphism in T_{reg} cells in the VAT. Male VAT was enriched for T_{reg} cells compared with female VAT, and T_{reg} cells from male VAT were markedly different from their female counterparts in phenotype, transcriptional landscape and chromatin accessibility. Heightened inflammation in the male VAT facilitated the recruitment of T_{reg} cells via the CCL2–CCR2 axis. Androgen regulated the differentiation of a unique IL-33-producing stromal cell population specific to the male VAT, which paralleled the local expansion of T_{reg} cells. Sex hormones also regulated VAT inflammation, which shaped the transcriptional landscape of VAT-resident T_{reg} cells in a BLIMP1 transcription factor-dependent manner. Overall, we find that sex-specific differences in T_{reg} cells from VAT are determined by the tissue niche in a sex-hormone-dependent manner to limit adipose tissue inflammation.

Sex-dependent differences in adipose tissue physiology and organismal metabolism are well documented across species[10,11]. Consistent with this notion, male and female mice display differences in body weight, ratio of lean mass to fat mass and rates of energy expenditure (Fig. 1a, b, Extended Data Fig. 1a–c). Males compared with age-matched females show relative glucose intolerance and concomitant hyperinsulinaemia, hallmarks of insulin resistance, but no differences in adipokines (Fig. 1c, Extended Data Fig. 1d, e). Immune cells have critical roles in VAT-mediated regulation of organismal metabolism[12–17]. Analysis of perigonadal VAT of lean male mice revealed much larger proportions and numbers of T_{reg} cells compared with those from female mice (Fig. 1d–f). This difference was specific to T_{reg} cells, as there were no significant differences between any other major adaptive and innate immune cell populations, including type 2 innate lymphocytes (ILC2s), which together with T_{reg} cells have an important role in VAT homeostasis[14,15,18,19] (Extended Data Fig. 1f, g). VAT T_{reg} cells also displayed marked sex-dependent phenotypic differences. While T_{reg} cells from VAT of both males and females had an activated phenotype ($CD62L^{-}CD44^{+}$), only those from males expressed high levels of the IL-33 receptor ST2, the maturation marker KLRG1 and the chemokine receptor CCR2 (Fig. 1g, Extended Data Fig. 1h). Likewise, the immune suppressive cytokine IL-10 was abundant in VAT T_{reg} cells from males but not in those from females (Fig. 1h). Sex-specific differences in T_{reg} cells were specific to the VAT, as abundance and IL-10 expression of T_{reg} cells in other lymphoid or non-lymphoid tissues, such as small intestine lamina propria, colon, liver and lung were similar (Extended Data Figs. 1i, 2a). Furthermore, the differences were specific to the adipose tissue depot, as neither the subcutaneous nor the perinephric adipose tissue showed sex-specific differences in abundance or phenotype of T_{reg} cells (Extended Data Fig. 2b, c).

Sex-specific VAT T_{reg} cell molecular profile

To gain insight into the molecular mechanisms that underpin the sex-dependent differences in VAT T_{reg} cells, we compared transcriptional profiles of T_{reg} cells isolated from the VAT and spleens of male and female mice by RNA sequencing (RNA-seq). T_{reg} cells isolated from male VAT and spleen differed substantially, revealing a distinct VAT T_{reg} cell transcriptional signature of almost 3,000 genes (false discovery rate 0.1,

[1]Department of Microbiology and Immunology, The Peter Doherty Institute for Infection and Immunity, University of Melbourne, Melbourne, Victoria, Australia. [2]The Walter and Eliza Hall Institute of Medical Research, Melbourne, Victoria, Australia. [3]Department of Medical Biology, University of Melbourne, Melbourne, Victoria, Australia. [4]Peter MacCallum Cancer Centre, Melbourne, Victoria, Australia. [5]College of Health and Medicine, School of Health Sciences, University of Tasmania, Launceston, Tasmania, Australia. [6]Institute of Experimental Immunology, University of Bonn, Bonn, Germany. [7]Monash Institute of Pharmaceutical Sciences, Parkville, Victoria, Australia. [8]Department of Immunology, Harvard Medical School, Boston, MA, USA. [9]Department of Medicine, Austin Health, The University of Melbourne, Melbourne, Victoria, Australia. [10]Department of Computing and Information Systems, The University of Melbourne, Melbourne, Victoria, Australia. ✉e-mail: ajith.vasanthakumar@unimelb.edu.au; axel.kallies@unimelb.edu.au

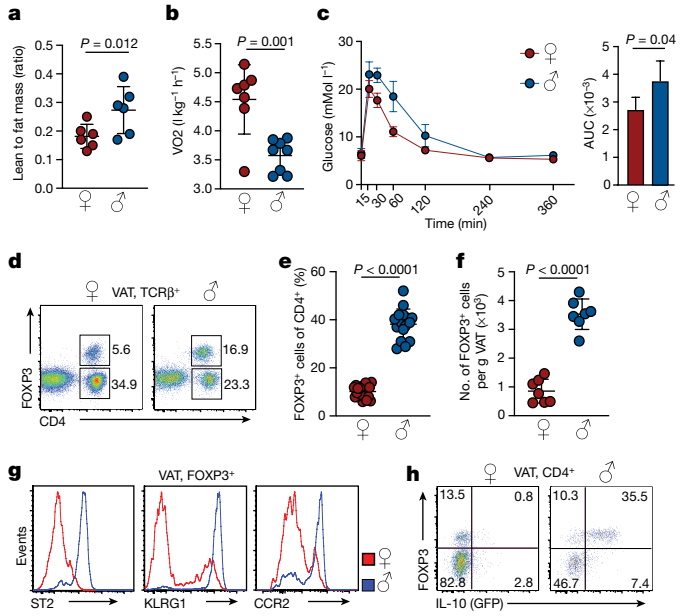

Fig. 1 | T_{reg} cells show VAT-specific sexual dimorphism. a, Ratio of lean mass to fat mass. Female, $n = 6$; male, $n = 6$. **b**, Oxygen consumption. Female, $n = 7$; male, $n = 8$. **c**, Glucose tolerance in 25-week-old female and male mice under normal chow diet conditions. $n = 4$ mice of each sex. Graph on the right shows area under the curve (AUC) for the glucose-tolerance test. **d**, Proportions of FOXP3$^+$ cells among T cell receptor β (TCRβ)-positive T cells in VAT of female and male C57BL/6 mice. Representative of $n = 19$ females and $n = 16$ males. **e**, FOXP3$^+$ T_{reg} cells as a proportion of CD4$^+$ cells. Female, $n = 19$; male, $n = 16$. **f**, T_{reg} cell numbers in the VAT of female and male mice. $n = 7$ mice of each sex. **g**, Expression of indicated cell surface markers on male and female VAT T_{reg} cells. Representative of $n = 19$ females and $n = 16$ males. **h**, *Il10* (GFP) expression in T_{reg} cells in VAT from male and female *Foxp3*^{RFP}*Il10*^{GFP} mice. Representative of $n = 6$ mice of each sex. Two-tailed unpaired *t*-test (**a**–**c**, **e**, **f**); data are mean ± s.d. Data pooled or representative of two or three independent experiments.

fold change >2) (Fig. 2a, Supplementary Information). By contrast, T_{reg} cells from female VAT were similar to their splenic counterparts, with only 305 differentially expressed genes (Fig. 2b, Supplementary Information). Comparison of male and female VAT T_{reg} cells revealed large differences in their transcriptional profiles, with >1,100 genes differentially expressed between the sexes; splenic T_{reg} cells showed no such differences (Fig. 2c, Extended Data Fig. 2d, Supplementary Information). In line with our flow-cytometric data, male VAT T_{reg} cells showed higher expression of *Il1rl1* (encoding ST2), *Il10*, *Ccr2* and *Klrg1*. Similarly, male but not female VAT T_{reg} cells expressed high amounts of *Pparg* (required for VAT T_{reg} cell differentiation[20]), *Prdm1* (encoding BLIMP1, associated with effector T_{reg} cell differentiation[21]) and *Gata3*. By contrast, female VAT T_{reg} cells showed increased amounts of *Sell* (encoding CD62L), *Cxcr5*, *Stat1*, *Foxo1* and *Tcf7* (Fig. 2c). Far fewer genes, including the ubiquitous male-specific *Ddx3y* and female-specific *Xist*, were differentially expressed between male and female VAT-resident ILC2s and conventional CD4$^+$ T cells (Extended Data Fig. 2e, f, Supplementary Information), indicating that the sex-dependent differences in gene expression were specific to VAT T_{reg} cells. To test whether the distinct transcriptional profiles of male and female VAT T_{reg} cells were reflected in differential chromatin accessibility, we performed assay for transposase-accessible chromatin using sequencing (ATAC-seq) (Fig. 2d). We found 3,833 loci with sex-dependent differential accessibility in VAT T_{reg} cells. This included *Il1rl1*, *Il10*, *Pparg* and *Klrg1*, which were part of the male VAT T_{reg} cell transcriptional signature and showed increased accessibility in male VAT T_{reg} cells compared with both female VAT T_{reg} and male splenic T_{reg} cells (Fig. 2e, Extended Data Fig. 2g, h, Supplementary Information).

T_{reg} cell extrinsic sex-hormonal function

Sex hormones are central to many developmental processes and are enriched in adipose tissue[22]. To test whether VAT T_{reg} cells were regulated by sex hormones, we analysed mice that were deficient for either androgen or oestrogen receptors. VAT T_{reg} cells from male mice lacking the androgen receptor (*Ar*$^{-/-}$) were significantly reduced compared to their wild-type counterparts and displayed a phenotype similar to female wild-type VAT T_{reg} cells, including diminished ST2, KLRG1 and CCR2 expression (Fig. 3a–c, Extended Data Fig. 3a). By contrast, female but not male mice lacking oestrogen receptor-α (*Era*$^{-/-}$, also known as *Esr1*$^{-/-}$) showed a significant increase in VAT T_{reg} cells that displayed the phenotype of male VAT T_{reg} cells with elevated expression of ST2, KLRG1 and CCR2 (Fig. 3d–f, Extended Data Fig. 3b, c). This phenotype was recapitulated when we treated female wild-type mice with ICI 182-780, an oestrogen receptor antagonist (Extended Data Fig. 3d, e). Consistent with an important role of sex hormones in VAT physiology, male *Ar*$^{-/-}$ mice had reduced VAT mass and improved glucose tolerance, whereas female *Era*$^{-/-}$ mice had increased VAT mass and decreased glucose tolerance (Extended Data Fig. 3f–i). Both *Ar*$^{-/-}$ and *Era*$^{-/-}$ mice showed modestly increased fasting plasma insulin compared with controls (Extended Data Fig. 3j, k).

Sex hormone receptors are widely expressed, including by cells of the immune system[23,24]. To test whether the functions of hormone receptors are intrinsic to T_{reg} cells, we generated bone marrow chimeric mice by transferring congenically marked male wild-type bone marrow into lethally irradiated male *Ar*$^{-/-}$ or wild-type recipients (Extended Data Fig. 4a). Male wild-type VAT T_{reg} cells that developed in an androgen receptor-deficient environment acquired the phenotype typical for female VAT T_{reg} cells, whereas they adopted the male phenotype in a wild-type environment (Extended Data Fig. 4b, c), indicating that sexual dimorphism of VAT T_{reg} cells is extrinsic. This notion was confirmed when we generated *Ar*$^{fl/fl}$*Foxp3*^{cre} mice, in which the androgen receptor was deleted specifically in T_{reg} cells (Extended Data Fig. 4d, e). Consistent with a T_{reg} cell-extrinsic activity of oestrogen, oestrogen receptor-deficient and wild-type T_{reg} cells were represented equally in mixed bone marrow chimeric mice containing congenically marked wild-type and *Era*$^{-/-}$ haematopoietic cells (Extended Data Fig. 4f). Finally, treatment of male wild-type mice with oestrogen resulted in a decrease in T_{reg} cells specifically in the VAT and reduced KLRG1 and ST2 expression, whereas female wild-type mice treated with testosterone showed an increase in these parameters (Fig. 3g, Extended Data Fig. 4g–l). Overall, our data show that a sex hormone-dependent niche enforces the VAT T_{reg} cell-specific phenotype.

VAT inflammation recruits T_{reg} cells

To examine the nature of the sex-specific T_{reg} cell niche in the VAT, we performed RNA-seq analysis of total VAT and subcutaneous adipose tissue from male and female mice. We observed substantial differences between adipose tissue from different depots. Compared with subcutaneous adipose tissue, the VAT was enriched in proinflammatory genes including *Ccl2*, *Tnf* and *Il1b* as well as *Il33* (Fig. 3h, Supplementary Information). VAT displayed substantial sex-dependent transcriptional differences, with nearly 1,300 genes differentially expressed between tissues isolated from male and female mice (Fig. 3i, Extended Data Fig. 5a, Supplementary Information). In particular, the expression of genes that contribute to inflammation (*Tnf*, *Ccl2* and *Il1b*), tissue fibrosis (*Col6a5*) and prostaglandin metabolism (*Hpgds*) was elevated in male VAT compared with female VAT. As T_{reg} cells from male VAT express high levels of CCR2, the high expression of its ligand, CCL2 (also known as MCP-1), in male VAT was of particular interest. To understand the T_{reg} cell-intrinsic role of CCR2 in the VAT, we generated mixed bone marrow chimeric mice containing both CCR2-deficient (*Ccr2*$^{-/-}$) and wild-type haematopoietic cells. In male chimeric mice, we observed

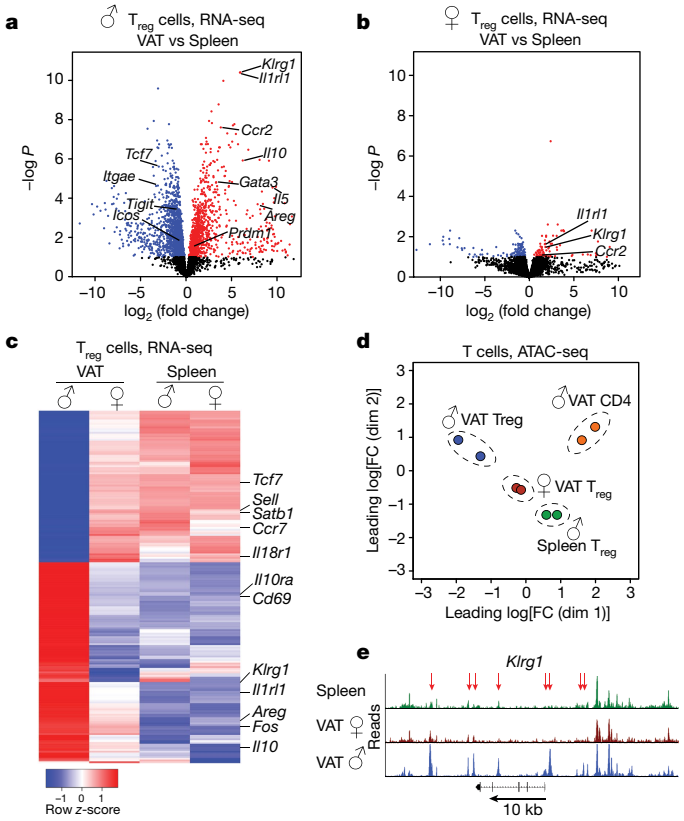

Fig. 2 | T_{reg} cells from male and female VAT exhibit distinct transcriptional profiles and chromatin accessibility. T_{reg} cells were sorted from VAT and spleens of 25- to 32-week-old *Foxp3*^{RFP} mice to perform RNA-seq and ATAC-seq. $n = 2$ samples, each sample contains T_{reg} cells from $n = 5$ male and $n = 12$ female mice. **a**, Volcano plot shows genes differentially expressed between T_{reg} cells from male VAT and spleen. Each dot represents a gene; genes in red are upregulated and genes in blue are downregulated in T_{reg} cells from VAT of male mice. **b**, Volcano plot shows genes differentially expressed between T_{reg} cells from female VAT and spleen. Genes in red are upregulated and genes in blue are downregulated in T_{reg} cells from VAT of female mice. **c**, Heat map shows top-200 genes that are differentially expressed between male and female VAT and comparison with splenic T_{reg} cells. **d**, Multi-dimensional scaling analysis of ATAC-seq data. Distances shown on the plot represent the leading $\log_2$ fold change between samples. **e**, ATAC-seq tracks show chromatin accessibility at the *Klrg1* locus of male splenic T_{reg} cells (green) and T_{reg} cells from female (red) and male (blue) VAT. Arrows indicate regions of differential chromatin accessibility. Statistical methods and software packages are described in Methods.

a reduction of *Ccr2*$^{-/-}$ VAT T_{reg} cells compared with wild-type cells as well as reduced expression of prototypical VAT T_{reg} cell markers. This defect was restricted to the VAT, as spleens or small intestines contained similar proportions of *Ccr2*$^{-/-}$ and wild-type T_{reg} cells (Fig. 3j, Extended Data Fig. 5b, c). The difference was specific to T_{reg} cells, as ILC2s of either genotype were similarly represented in the VAT of chimeric mice (Extended Data Fig. 5d). By contrast, mice deficient in TNF, IL-1β and IFNγ showed no substantial loss or altered phenotype of VAT T_{reg} cells (Extended Data Fig. 5e). Notably, a small fraction of T_{reg} cells in the spleens of both male and female mice co-expressed KLRG1 and CCR2, and these cells could be expanded by administration of IL-33 (Extended Data Fig. 5f–h). This suggested that VAT T_{reg} cells were recruited from splenic precursors, a notion consistent with recent work[25] and long-term parabiosis experiments, which showed that T_{reg} cells—unlike ILC2s—are continuously recruited to the VAT (Extended Data Fig. 5i–k). In line with a critical role for sex hormones in regulating the abundance of inflammatory mediators in the VAT, expression of *Ccl2*, *Il1b* and *Il6* was higher in female *Era*$^{-/-}$ VAT compared with wild-type controls (Fig. 3k). Similarly, female mice treated with testosterone showed an increase in the expression of *Il6*, *Ccl2* and *Il1b* in the VAT and increased VAT weight, whereas male mice treated with oestrogen showed reductions in these parameters (Extended Data Fig. 6a, b). Finally, treatment of male mice with celecoxib, a pharmacological inhibitor of cyclooxygenase-2 (COX2), reduced the amount of inflammatory mediators such as CCL2 and the abundance of VAT T_{reg} cells in male mice (Extended Data Fig. 6c–e). Together, these results show that T_{reg} cells use the same molecular cues as pro-inflammatory cells to populate the adipose tissue and are recruited to the male VAT in a manner dependent on CCL2 and limited by oestrogen.

Sex hormones control IL-33$^+$ stromal cells

To characterize the tissue niche that imparts the phenotypic and molecular features of VAT T_{reg} cells, we performed RNA-seq analysis of adipocytes, endothelial cells (CD31$^+$Gp38$^-$) and stromal cells (CD31$^-$Gp38$^+$) isolated from the VAT of male and female mice (Extended Data Fig. 6f, Supplementary Information). We first identified the source of IL-33, which acts as a critical growth factor that facilitates expansion of VAT T_{reg} cells[26,27]. Consistent with recent reports[13,28–30], *Il33* expression was largely restricted to Gp38$^+$ stromal cells, which were present in males and females in similar numbers (Extended Data Fig. 6g, i). However, Gp38$^+$ cells of males and females showed marked differences in their transcriptional profiles, including elevated expression of *Nt5e* (encoding the ecto-nucleotidase CD73) in males, whereas *Cd90*—encoding a marker of mesenchymal stromal cells—was downregulated (Extended Data Fig. 6h). Differential expression of CD90 and CD73 segregated four distinct Gp38$^+$ stromal cell populations, of which the two that expressed CD73$^+$ were largely restricted to the male VAT and almost absent from other adipose tissue depots and from females (Fig. 4a, b, Extended Data Fig. 6j). Analysis of *Il33*^{GFP} reporter mice revealed that IL-33 production was restricted to Gp38$^+$ stromal cells, including the CD73$^+$ fraction (Fig. 4c, d, Extended Data Fig. 7a). Indeed, we detected fewer IL-33-producing stromal cells in female VAT compared with male VAT (Extended Data Fig. 7b, c). Consistent with the idea that IL-33 is limiting in female mice, administration of IL-33 led to robust expansion of female VAT T_{reg} cells, which proliferated locally in the VAT and upregulated ST2 (Extended Data Fig. 7d–h). Further supporting this model, T_{reg} cells sorted from the spleens of transgenic mice expressing a VAT-specific T cell receptor[25] and transferred into congenically marked mice, populated the VAT of male mice more efficiently and expressed higher amounts of ST2 compared with T_{reg} cells transferred into female mice (Extended Data Fig. 7i). Male *Ar*$^{-/-}$ mice had significantly fewer CD73$^+$ stromal cells, whereas female *Era*$^{-/-}$ mice had more CD73$^+$ stromal cells compared with their wild-type counterparts, suggesting that the development of these cells is supported by sex hormones (Fig. 4e, f). Indeed, treatment of female mice with testosterone resulted in the induction of CD73$^+$ stromal cells, whereas treatment of male mice with oestrogen resulted in a reduction in the number of these cells (Fig. 4g, h, Extended Data Fig. 8a, b). Administration of IL-33 to *Ar*$^{-/-}$ mice resulted in pronounced population expansion of VAT T_{reg} cells, suggesting that IL-33 is limiting in these mice (Extended Data Fig. 8c). By contrast, treatment of male mice with celecoxib resulted in an increase in CD73$^+$ stromal cells (Extended Data Fig. 8d), indicating that the reduction of VAT T_{reg} cells in celecoxib-treated mice was not linked to the loss of IL-33-producing stromal cells. Together these experiments reveal that sex hormones regulate the development of specific IL-33-producing stromal cell populations and show that IL-33 availability controls the size of the VAT T_{reg} cell niche.

BLIMP1 controls VAT T_{reg} cell genes

Finally, to elucidate how the VAT T_{reg} cell-specific transcriptional landscape is shaped in a T_{reg} cell intrinsic manner, we tested the function of

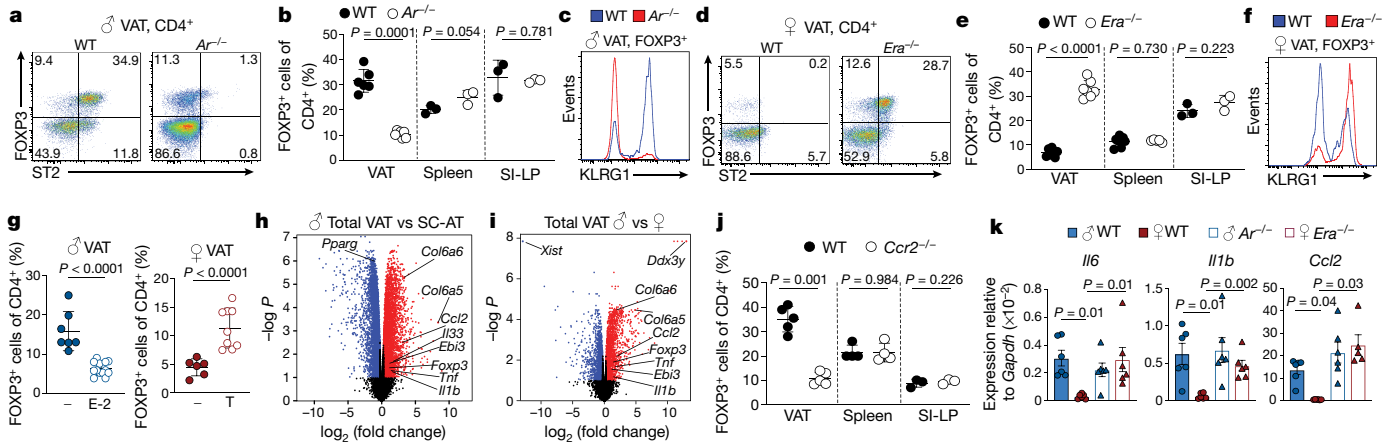

Fig. 3 | Sex differences in VAT T_{reg} cells are linked to sex hormones. a, FOXP3 and ST2 expression in $CD4^+$ T cells from VAT of male wild-type (WT) and $Ar^{-/-}$ mice. Wild type, $n = 6$; $Ar^{-/-}$, $n = 7$. **b**, $FOXP3^+$ cells among $CD4^+$ T cells in VAT ($n = 6$ wild type, $n = 7$ $Ar^{-/-}$), spleen and small intestine lamina propria (SI-LP) of wild-type and $Ar^{-/-}$ male mice. $n = 3$ mice per genotype. **c**, KLRG1 expression in T_{reg} cells from VAT of wild-type and $Ar^{-/-}$ male mice. Wild type, $n = 6$; $Ar^{-/-}$, $n = 7$. **d**, FOXP3 and ST2 expression in VAT $CD4^+$ T cells from female wild-type and $Era^{-/-}$ mice. Wild type, $n = 6$; $Era^{-/-}$, $n = 7$. **e**, $FOXP3^+$ T_{reg} cells among $CD4^+$ T cells from wild-type and $Era^{-/-}$ mice; VAT ($n = 6$ wild type, $n = 7$ $Era^{-/-}$), spleen ($n = 7$ wild type, $n = 5$ $Era^{-/-}$) and SI-LP ($n = 3$ per genotype). **f**, KLRG1 expression in T_{reg} cells from VAT of female wild-type and $Era^{-/-}$ mice. Wild type, $n = 6$; $Era^{-/-}$, $n = 7$. **g**, Left, percentage of $FOXP3^+$ T_{reg} cells in VAT from mock-treated ($n = 7$) and oestrogen-treated (E-2) male wild-type mice ($n = 13$). Right, as left, but for mock-treated ($n = 6$) and testosterone (T)-treated ($n = 9$) female wild-type mice. **h**, **i**, Volcano plot showing genes differentially expressed between male VAT and subcutaneous adipose tissue (SC-AT) (**h**), or between total male and female VAT (**i**). Each dot represents a gene; genes in red are upregulated and genes in blue are downregulated in the respective comparison. **j**, Proportion of T_{reg} cells in the wild-type and $Ccr2^{-/-}$ compartments of the VAT ($n = 5$), spleen ($n = 4$) and SI-LP ($n = 3$) of male mixed bone marrow chimeric mice. **k**, Quantitative PCR analysis of gene expression in age-matched male wild-type and $Ar^{-/-}$ and female wild-type and $Era^{-/-}$ mice. Two-tailed unpaired *t*-test (**b**, **e**, **g**, **j**); one-way analysis of variance (ANOVA) (**k**). Data are mean ± s.d., except in **k**, mean ± s.e.m. Data are pooled or representative of two independent experiments.

the transcription factor BLIMP1, which was increased in VAT T_{reg} cells from male mice compared with those from female mice (Extended Data Fig. 8e). Male $Blimp1^{fl/fl}Foxp3^{cre}$ mice, which lack BLIMP1 specifically in T_{reg} cells, exhibited reduced numbers of VAT T_{reg} cells, which showed lower ST2, KLRG1, TIGIT and CCR2 expression, and upregulated CD103 and CD62L expression (Fig. 4i, j, Extended Data Fig. 8f). Consistent with a loss of VAT T_{reg} cells, male $Blimp1^{fl/fl}Foxp3^{cre}$ mice showed reduced glucose tolerance (Extended Data Fig. 8g). RNA-seq revealed more than 2,500 genes deregulated in BLIMP1-deficient VAT T_{reg} cells compared with control cells, including downregulation of VAT T_{reg} signature genes *Il1rl1*, *Klrg1*, *Ccr2*, *Pparg* and *Il10*, resulting in a transcriptional profile similar to that of female VAT T_{reg} cells (Extended Data Fig. 9a, b, Supplementary Information). To identify direct targets of BLIMP1, we interrogated our ATAC-seq data and previously published BLIMP1

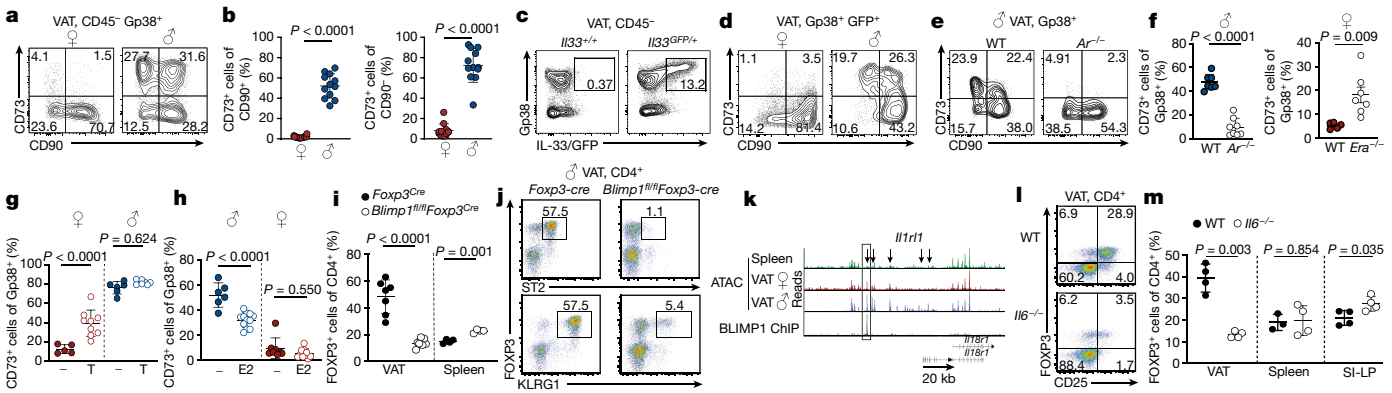

Fig. 4 | Hormone-dependent stromal cells and BLIMP1 underpin VAT T_{reg} cell sexual dimorphism. a, CD90 and CD73 expression in $Gp38^+$ VAT stromal cells from C57BL/6 female and male mice. **b**, Percentage of $CD73^+$ cells of $CD90^+$ (left) and $CD90^-$ (right) cells. $n = 12$ mice of each sex. **c**, *Il33* (GFP) and Gp38 expression in $CD45^-$ VAT stromal vascular fraction from male wild-type and $Il33^{GFP}$ mice. Representative of $n = 6$ mice. **d**, CD73 and CD90 expression in $Gp38^+$*Il33* $(GFP)^+$ VAT stromal cells from male and female $Il33^{GFP}$ mice. Representative of $n = 8$ of both sexes. **e**, CD73 and CD90 expression within $Gp38^+$ stromal cells from male wild-type and $Ar^{-/-}$ VAT. **f**–**h**, Proportions of $CD73^+$ cells within $Gp38^+$ VAT stromal cells of wild-type ($n = 7$) and $Ar^{-/-}$ ($n = 8$) males (**f**, left), wild-type ($n = 5$) and $Era^{-/-}$ ($n = 7$) females (**f**, right), C57BL/6 mice treated with testosterone (T) ($n = 9$ females treated, $n = 5$ females untreated, $n = 8$ males treated, $n = 6$ males untreated) (**g**) and C57BL/6 mice treated with oestrogen (E2) ($n = 12$ males treated, $n = 6$ males untreated, $n = 10$ females treated, $n = 8$ females untreated) (**h**). **i**, Proportions of T_{reg} cells in the VAT ($n = 7$ per genotype) and spleens ($n = 4$ per genotype) of $Blimp1^{fl/fl}Foxp3^{cre}$ and $Foxp3^{cre}$ mice. **j**, Expression of FOXP3, ST2 and KLRG1 in VAT $CD4^+$ T cells from $Blimp1^{fl/fl}Foxp3^{cre}$ and $Foxp3^{cre}$ control mice. **k**, ATAC-seq tracks show chromatin accessibility (male spleen, green; female VAT, red; male VAT, blue) and ChIP–seq shows BLIMP1 occupancy (black) in the *Il1rl1* locus. Arrows indicate differential accessibility and boxes indicate BLIMP1-occupied sites. **l**, Flow cytometry plots show expression of FOXP3 and CD25 in VAT $CD4^+$ T cells from wild-type and $Il6^{-/-}$ mice. **m**, Proportions of splenic, VAT and small intestine lamina propria (SI-LP) T_{reg} cells among VAT $CD4^+$ T cells of wild-type and $Il6^{-/-}$ mice ($n = 4$ per genotype). Two-tailed unpaired *t*-test; data are mean ± s.d. Data are pooled or representative of two independent experiments.

chromatin immunoprecipitation with sequencing (ChIP–seq) data[31]. In total, we detected 2,095 ChIP peaks that overlapped with open chromatin in VAT T_{reg} cells. These sites were associated with BLIMP1 target genes such as *Ccr7*, *Tcf7*, *Klf2*, *Cxcr5*, *S1pr1*, *Myc* and *Bcl6*, and key genes of the VAT T_{reg} cell signature, including *Il10*, *Ccr2* and *Il1rl1*, suggesting that these genes were direct transcriptional targets of BLIMP1 in VAT T_{reg} cells (Extended Data Fig. 9c, d, Supplementary Information). BLIMP1-binding sites were detected in multiple loci with differential accessibility in splenic T_{reg} cells and male and female VAT T_{reg} cells, respectively. This included sites in *Il1rl1*, which showed full accessibility in male VAT T_{reg} cells but reduced accessibility in female VAT T_{reg} cells and was fully closed in splenic T_{reg} cells (Fig. 4k). Notably, $CCR2^+KLRG1^+$ splenic T_{reg} cells also expressed BLIMP1 and *Pparg*, and loss of BLIMP1 resulted in a loss of CCR2 expression and an overall reduction of $KLRG1^+$ T_{reg} cells (Extended Data Fig. 10a–e). IL-6 and IL-4, both abundant in the VAT, potently induced BLIMP1 in T_{reg} cells in vitro, whereas IL-33 did not (Extended Data Fig. 10f). *Il6* was mainly expressed by VAT dendritic cells, macrophages and ILC2s (Extended Data Fig. 10g). Consistent with an important role for IL-6 in VAT physiology, $CD73^+$ stromal cells, T_{reg} cells and ILC2s were reduced in the VAT of male IL-6-deficient mice, and VAT T_{reg} cells showed impaired expression of ST2, KLRG1 and CCR2 (Fig. 4l, m, Extended Data Fig. 10h–j). Administration of IL-33 to IL-6-deficient mice resulted in pronounced population expansion of VAT T_{reg} cells, suggesting that IL-6 per se is not essential for the differentiation of VAT T_{reg} cells but promotes the availability of IL-33 (Extended Data Fig. 10k).

The VAT constitutes an inflammatory environment, and low-grade inflammation—which increases in obesity—contributes to the development of metabolic disease and type 2 diabetes. Our data show that in females, inflammation is limited by oestrogen. In males, however, increased VAT inflammation and male-specific IL-33-producing stromal cells mediate the active recruitment and local expansion of T_{reg} cell numbers in a BLIMP1-dependent manner. This pathway constitutes a male-specific feedback circuit that limits inflammation in the VAT (Extended Data Fig. 10l).

Online content

Any methods, additional references, Nature Research reporting summaries, source data, extended data, supplementary information, acknowledgements, peer review information; details of author contributions and competing interests; and statements of data and code availability are available at https://doi.org/10.1038/s41586-020-2040-3.

1. Meseguer, A., Puche, C. & Cabero, A. Sex steroid biosynthesis in white adipose tissue. *Horm. Metab. Res.* **34**, 731–736 (2002).
2. Kamat, A., Hinshelwood, M. M., Murry, B. A. & Mendelson, C. R. Mechanisms in tissue-specific regulation of estrogen biosynthesis in humans. *Trends Endocrinol. Metab.* **13**, 122–128 (2002).
3. Luo, L. & Liu, M. Adipose tissue in control of metabolism. *J. Endocrinol.* **231**, R77–R99 (2016).
4. Rosen, E. D. & Spiegelman, B. M. Adipocytes as regulators of energy balance and glucose homeostasis. *Nature* **444**, 847–853 (2006).
5. Mraz, M. & Haluzik, M. The role of adipose tissue immune cells in obesity and low-grade inflammation. *J. Endocrinol.* **222**, R113–R127 (2014).
6. Cildir, G., Akıncılar, S. C. & Tergaonkar, V. Chronic adipose tissue inflammation: all immune cells on the stage. *Trends Mol. Med.* **19**, 487–500 (2013).
7. Josefowicz, S. Z., Lu, L. F. & Rudensky, A. Y. Regulatory T cells: mechanisms of differentiation and function. *Annu. Rev. Immunol.* **30**, 531–564 (2012).
8. Ohkura, N., Kitagawa, Y. & Sakaguchi, S. Development and maintenance of regulatory T cells. *Immunity* **38**, 414–423 (2013).
9. Panduro, M., Benoist, C. & Mathis, D. Tissue T_{reg}s. *Annu. Rev. Immunol.* **34**, 609–633 (2016).
10. White, U. A. & Tchoukalova, Y. D. Sex dimorphism and depot differences in adipose tissue function. *Biochim. Biophys. Acta* **1842**, 377–392 (2014).
11. Karastergiou, K., Smith, S. R., Greenberg, A. S. & Fried, S. K. Sex differences in human adipose tissues - the biology of pear shape. *Biol. Sex Differ.* **3**, 13 (2012).
12. Feuerer, M. et al. Lean, but not obese, fat is enriched for a unique population of regulatory T cells that affect metabolic parameters. *Nat. Med.* **15**, 930–939 (2009).
13. Kohlgruber, A. C. et al. γδ T cells producing interleukin-17A regulate adipose regulatory T cell homeostasis and thermogenesis. *Nat. Immunol.* **19**, 464–474 (2018).
14. Lee, M. W. et al. Activated type 2 innate lymphoid cells regulate beige fat biogenesis. *Cell* **160**, 74–87 (2015).
15. Molofsky, A. B. et al. Interleukin-33 and interferon-γ counter-regulate group 2 innate lymphoid cell activation during immune perturbation. *Immunity* **43**, 161–174 (2015).
16. Wensveen, F. M. et al. NK cells link obesity-induced adipose stress to inflammation and insulin resistance. *Nat. Immunol.* **16**, 376–385 (2015).
17. Lynch, L. et al. Regulatory iNKT cells lack expression of the transcription factor PLZF and control the homeostasis of T_{reg} cells and macrophages in adipose tissue. *Nat. Immunol.* **16**, 85–95 (2015).
18. Moro, K. et al. Innate production of T_H2 cytokines by adipose tissue-associated $c\text{-}Kit^+Sca\text{-}1^+$ lymphoid cells. *Nature* **463**, 540–544 (2010).
19. Brestoff, J. R. et al. Group 2 innate lymphoid cells promote beiging of white adipose tissue and limit obesity. *Nature* **519**, 242–246 (2015).
20. Cipolletta, D. et al. PPAR-γ is a major driver of the accumulation and phenotype of adipose tissue T_{reg} cells. *Nature* **486**, 549–553 (2012).
21. Cretney, E. et al. The transcription factors Blimp-1 and IRF4 jointly control the differentiation and function of effector regulatory T cells. *Nat. Immunol.* **12**, 304–311 (2011).
22. Michalakis, K., Mintziori, G., Kaprara, A., Tarlatzis, B. C. & Goulis, D. G. The complex interaction between obesity, metabolic syndrome and reproductive axis: a narrative review. *Metabolism* **62**, 457–478 (2013).
23. Kissick, H. T. et al. Androgens alter T-cell immunity by inhibiting T-helper 1 differentiation. *Proc. Natl Acad. Sci. USA* **111**, 9887–9892 (2014).
24. Kovats, S. Estrogen receptors regulate innate immune cells and signaling pathways. *Cell. Immunol.* **294**, 63–69 (2015).
25. Li, C. et al. TCR transgenic mice reveal stepwise, multi-site acquisition of the distinctive fat-T_{reg} phenotype. *Cell* **174**, 285–299 (2018).
26. Vasanthakumar, A. et al. The transcriptional regulators IRF4, BATF and IL-33 orchestrate development and maintenance of adipose tissue-resident regulatory T cells. *Nat. Immunol.* **16**, 276–285 (2015).
27. Kolodin, D. et al. Antigen- and cytokine-driven accumulation of regulatory T cells in visceral adipose tissue of lean mice. *Cell Metab.* **21**, 543–557 (2015).
28. Mahlakõiv, T. et al. Stromal cells maintain immune cell homeostasis in adipose tissue via production of interleukin-33. *Sci. Immunol.* **4**, eaax0416 (2019).
29. Spallanzani, R. G. et al. Distinct immunocyte-promoting and adipocyte-generating stromal components coordinate adipose tissue immune and metabolic tenors. *Sci. Immunol.* **4**, eaaw3658 (2019).
30. Koga, S. et al. Peripheral $PDGFR\alpha^+gp38^+$ mesenchymal cells support the differentiation of fetal liver-derived ILC2. *J. Exp. Med.* **215**, 1609–1626 (2018).
31. Mackay, L. K. et al. Hobit and Blimp1 instruct a universal transcriptional program of tissue residency in lymphocytes. *Science* **352**, 459–463 (2016).

Methods

No statistical methods were used to predetermine sample size. The experiments were not randomized. The investigators were not blinded to allocation during experiments and outcome assessment.

Mice

Era$^{-/-}$ (Jax stock no. 026176), *Ar*$^{-/-}$ (ref. [32]), *Ar*$^{fl/fl}$ (ref. [33]), *Ccr2*$^{-/-}$ (Jax stock no. 004999), *Blimp1*$^{fl/fl}$ (ref. [34]), *Blimp1*^{GFP} (ref. [35]), *Il33*^{GFP} (Jax stock no. 002650), *Il6*$^{-/-}$ (Jax stock no. 002650), *Tnf*$^{-/-}$ (Jax stock no. 003008), *Il1b*$^{-/-}$ (ref. [36]), *Rag1*$^{-/-}$ (Jax stock no. 002216) and C57BL/6 Ly5.1 mice were bred at the The Walter and Eliza Hall Institute animal facility. *Foxp3*^{cre} (Jax stock no. 016961), *Foxp3*^{RFP} (Jax stock no. 008374) and *IL10*^{GFP} (Jax stock no. 014530) mice were purchased from the Jackson laboratory. All mouse lines were maintained on a C57BL/6J (Ly5.2) background, except *Il33*$^{-/-}$, which is on a C57BL/6N background. Mice were analysed at 25–30 weeks of age unless specified. Mice were maintained and used in accordance with the guidelines of the WEHI Animal Ethics Committee.

Bone marrow chimaeras

Bone marrow chimeric mice were generated by lethally irradiating recipient mice with twice with 550 röntgen (R) and reconstituting them with 1×10^7 congenically marked bone marrow cells. *Ccr2*$^{-/-}$/Ly5.1 mixed chimeric mice were made in *Rag1*$^{-/-}$ recipients irradiated twice with 350 R.

Antibodies and flow cytometry

Fluorochrome-conjugated antibodies directed against the following mouse antigens were used for analysis by flow cytometry. Antibodies, clone names and manufactures: Invitrogen or eBioscience, KLRG1 (2F1) FITC, BV711; Thy1.2 (30-H12) FITC; γδTCR (ebioGL3) FITC; CD25 (PC61.5) PEcy7; Gp38 (eBio8.1.1) PEcy7; KLRG1 (2F1) PEcy7; ST2 (RMST2-2) APC; Tigit (GIGD7) eFluor660; GITR APC; CD25 (PC61.5) APC; TCRβ (H57-597) PerCP Cy5.5; Foxp3 (FJK-16 s) eFluor450; Ly5.2 (104) eFluor450; Gata3 (TWAJ) PE; CD103 (2E7) PE and EOMES (Dan11mag) PerCPeFluor710; BD Biosciences, Ly5.2 (104) FITC; CD4 (GK1.5) BUV496; CD19 (1D3) BUV737; CD8a (53-6.7) BUV737; CD45.2 (104) BUV395; CD11b (M1/70) BUV737 and KLRG1 (2F1) BV711; BioLegend, CD45.1 (A20) FITC; F4/80 (BM8) FITC; CD45.2 (104) BV605; CD4 (GK1.5) APC/cy7; CD11c (N418) BV711; CD69 (H1.2F3) BV711; F4/80 (BM8) BV605; CD140a (APA5) APC; CD31 (PacBlue) and CD73 (TY/11.8) PE; R&D Systems, mCCR2 A700; WEHI, NK1.1 (PK136) Alexa594. For surface staining, antibodies were diluted at 1:200 and incubated with cells in PBS with 2% BSA on ice or 4 °C for 30 min. The cell pellet was resuspended in live/dead stain containing PBS with 2% BSA. For intranuclear staining, a FOXP3 staining kit was used (Invitrogen).

Preparation of lymphocytes from adipose tissue

Unless indicated otherwise, perigonadal VAT was collected from 30- to 32-week-old male or female mice, finely minced and suspended in 0.025% collagenase type IV (Gibco) (2 ml collagenase per gram fat). The suspension was incubated for 45 min at 37 °C in a shaker. After incubation the suspension was 10 times diluted with PBS + 2% FCS and spun at 800*g* for 15 min at 4 °C. The upper adipocyte fraction was discarded and the stromal vascular fraction that settled down was further purified to obtain lymphocytes by Histopaque (Sigma) gradient.

Isolation of intestinal lamina propria lymphocytes

Lamina propria lymphocytes (LPLs) were extracted from the small intestine. In brief, Peyer's patches removed and intestines were opened longitudinally and cut into small pieces (<5 mm). Epithelial cells and intraepithelial lymphocytes were removed by washing with HBSS and incubating with 5 mM EDTA for 30 min at 37 °C. The intestinal pieces were washed with RPMI and 10% FCS, and LPLs were isolated by digestion with 1 μg ml^{-1} DNase (Sigma-Aldrich) and 200 μg ml^{-1} collagenase III (Worthington) for 40 min at 37 °C. The LPL fractions were purified with a 40–80% Percoll (GE Healthcare) gradient.

Parabiosis experiments

Mice were anaesthetized with ketamine and xylazine at 10 μg g^{-1}. Skin was shaved and disinfected by wiping with alcohol prep pads and betadine three times. Matching incisions were made from the olecranon to the knee joint of each mouse and subcutaneous fascia were bluntly dissected to create 0.5 cm of free skin. The olecranon and knee joints were attached by a 5-0 silk suture, and dorsal and ventral skin were attached by continuous staples or sutures. Betadine was used to cover the entire incision following surgery.

T_{reg} cell cultures

T_{reg} cells were purified from *Foxp3*^{RFP} mice by fluorescence-activated cell sorting. Sorted T_{reg} cells were cultured in 96-well flat-bottom plates with a density of 100,000 cells per well in 250 μl medium. Plates were pre-coated with anti-CD3 (2C11) (5 μg ml^{-1}) and T_{reg} cells were cultured in complete IMDM medium with IL-2 (100 U) and soluble anti-CD28 (2 μg ml^{-1}) along with other cytokines mentioned.

Adoptive transfer of T_{reg} cells

Five million CD4$^+$ T cells were purified from pooled spleen and lymph nodes of 6- to 8-week-old male or female CD45.2$^+$ vT_{reg}53 TCR Tg$^+$ littermates, using the Dynabeads Untouched Mouse CD4 Cells Kit (Thermo Fisher Scientific), and injected intravenously into sex-matched 6–8-week-old B6.CD45.1$^+$ mice. Engraftment and enrichment of donor-derived cells in the spleen, epididymal VAT, ovarian VAT or inguinal subcutaneous adipose tissue of recipient mice were analysed 12 weeks after transfer.

Glucose-tolerance tests

Glucose (1.75 g per kg of body weight) was injected intraperitoneally to mice fasted for 8 h. Blood samples were obtained from the tail tip at the indicated times, and blood glucose concentrations were measured using a handheld glucometer (Accu-Chek Performa, Roche).

Intracellular IL-33 staining

Intracellular IL-33 was detected by fixation and permeabilization using True-Nuclear Transcription Factor Buffer Set (BioLegend) as per the manufacturer's instructions followed by incubation with a goat anti–IL-33 polyclonal primary antibody (no. AF326, R&D Systems) and a donkey anti-goat Cy3 secondary antibody (no. 705-166-147, Jackson Immunoresearch Laboratories).

Celecoxib treatment

Seven-week-old male C57BL/6 were fed with celecoxib containing diet 29 mg kg^{-1} day^{-1} for 15 weeks.

Hormone treatment

Sixty-day release 0.25 mg 17-β oestradiol pellets (SE-121, Innovation Research of America) were surgically implanted subcutaneously in 7–8-week-old male and female C57BL/6 mice. For testosterone treatment, 4 mg testosterone (Sigma Aldrich, T1500) powder was packed in 1-cm silastic tubing and surgically implanted subcutaneously in 7–8-week-old male and female C57BL/6 mice. Mice were analysed six weeks post-implantation.

Serum adipokine and insulin measurement

Bio-Plex Pro mouse diabetes immunoassay kit (Bio Rad, 171F7001M) was used to measure fasting serum concentrations of adipokines according to the manufacturer's protocol. Adiponectin was measured with a separate kit from Bio Rad (Bio-Plex Pro Mouse Diabetes Adiponectin Assay Kit, 171F7001M).

ICI 182-780 treatment

For the oestrogen receptor antagonist experiments, adult C57BL/6 mice were ovariectomized and then either not treated any further or treated with 5 mg of ICI 182-780 (intraperitoneal injections, 1 per week for 6 weeks). At the end of the experiment, mice were collected and uterine weight used to confirm that ICI 182-780 treatment was successful.

Cytokine treatment

IL-33 (R&D systems) at 0.5 µg per head was administered intraperitoneally for 3 alternate days and mice were analysed on day 7. PBS was used as control.

High-fat diet

Male C57BL/6 mice were fed a high-fat diet in which 59% of the total energy is derived from lipids (59 kcal% fat, Specialty Feeds, SF03-002) for 40 weeks.

Echo MRI and indirect calorimetry

Body composition (fat and lean mass) was measured with a 4-in-1 EchoMRI body composition analyser (EchoMRI), and whole-body oxygen consumption was measured with a Comprehensive Laboratory Animal Monitoring System (Columbus Instruments) as previously described[37].

RNA extraction

RNA was extracted from VAT using Qiagen RNeasy lipid tissue mini kit as per the manufacturer's protocol. RNA from T_{reg} cells and stromal cells was isolated using Qiagen RNeasy plus micro kit as per the manufacturer's protocol. VAT was pooled from three mice per sample. VAT T_{reg} cells and stromal cells were sorted from pooled VAT from five or more mice. Stromal cells were sorted by flow cytometry as $Gp38^+$ or $Gp38^-$ from the $CD45^-Ter119^-$ population. Adipocytes were purified after removal of the stromal vascular fraction.

RNA-seq and analysis

Samples were generated from a male and female mouse respectively. All samples were sequenced on an Illumina NextSeq 500 generating 75 bp paired end reads. Reads were aligned to the mouse reference genome GRCm38/mm10 using the Subread aligner (v.1.6.2)[38]. Mapped reads were assigned to NCBI RefSeq mouse genes and genewise counts were produced by using featureCounts[39]. Genes that failed to achieve a CPM (counts per million mapped reads) value of 0.5 in at least 2 libraries were excluded from downstream analysis. Read counts were converted to $\log_2$ CPM, quantile-normalized and precision-weighted with the voom function of the limma package[40,41]. A linear model was fitted to each gene, and empirical Bayes-moderated *t*-statistics were used to assess differences in expression[42]. Genes were designated differentially expressed if they achieved a false discovery rate (FDR) less than 0.1 and a fold change greater than 1.2.

ATAC-seq and analysis

ATAC-seq was performed as described[43]. In brief, 35,000–50,000 T_{reg} cells were resuspended in 50 µl of chilled ATAC lysis buffer (10 mM TrisHCL, 10 mM NaCl, 3 mM $MgCl_2$ and 0.1% (v/v) Igepal CA-630) and centrifuged for 10 min at 500*g* at 4 °C. Nuclei of an equivalent of 25,000 cells were resuspended in 25 µl of Tagmentation buffer (2× Tagment DNA buffer, 20× Tagment DNA enzyme (Nexterea library preparation kit) and incubated at 37 °C for 30 min. Next, Tagmented DNA was isolated using the MinElute PCR purification kit (Qiagen). Samples were PCR-amplified with a common forward primer and unique barcoding reverse primers before tagmentation efficiency and concentration was assessed with a bioanalyzer high sensitivity DNA analysis kit (Agilent). Pooled libraries were cleaned from small (<150 bp) fragments and sequenced on a NextSeq 500 sequencer (Illumina) producing paired-end 75 bp reads. Sequence reads were mapped to mouse genome GRCm38/mm10 using Subread. Only uniquely mapped reads were retained. ATAC peaks were called using Homer (v.4.9) with a FDR cut-off of 10^{-5}. Overlapping peaks from different samples were merged into a single peak region that covers all the overlapping peaks. Mapped reads were assigned to all the merged regions for each sample using featureCounts. Regions were removed from analysis if they failed to achieve a CPM value of 0.7 or higher in at least one sample. Regions were annotated by assigning them to the nearest gene. Read counts for regions were converted to $\log_2$ CPM and precision-weighted with the limma voom function. A linear model was fitted to each region, and empirical Bayes moderated *t*-statistics were used to assess differences in chromatin accessibility. A FDR cut-off of 0.2 was applied for calling differentially accessed regions.

ChIP–seq analysis

BLIMP1 ChIP–seq reads were mapped to the mouse reference genome GRCm38/mm10 using the Subread aligner. BLIMP1 binding peaks were called using Homer (v.4.9) with a FDR cutoff of 10^{-4}. Peaks were assigned to their nearest gene. Overlapping peaks between ChIP–seq data and ATAC-seq data were identified as those that have at least 1 bp overlap.

Statistics

Unless specified otherwise, *t*-tests were performed to test for statistical significance and error bars denote mean ± s. d. unless specified.

Reporting summary

Further information on research design is available in the Nature Research Reporting Summary linked to this paper.

Data availability

Sequencing data generated for this study have been deposited in the Gene Expression Omnibus database with accession number GSE121838. Source data for Figs. 1, 3, 4 and Extended Data Figs. 1–8, 10 are available with the paper. All other data and materials are available upon request.

32. Notini, A. J., Davey, R. A., McManus, J. F., Bate, K. L. & Zajac, J. D. Genomic actions of the androgen receptor are required for normal male sexual differentiation in a mouse model. *J. Mol. Endocrinol*. **35**, 547–555 (2005).
33. Rana, K., Clarke, M. V., Zajac, J. D., Davey, R. A. & MacLean, H. E. Normal phenotype in conditional androgen receptor (AR) exon 3-floxed neomycin-negative male mice. *Endocr. Res*. **39**, 130–135 (2014).
34. Kallies, A., Xin, A., Belz, G. T. & Nutt, S. L. Blimp-1 transcription factor is required for the differentiation of effector $CD8^+$ T cells and memory responses. *Immunity* **31**, 283–295 (2009).
35. Kallies, A. et al. Plasma cell ontogeny defined by quantitative changes in blimp-1 expression. *J. Exp. Med*. **200**, 967–977 (2004).
36. Horai, R. et al. Production of mice deficient in genes for interleukin (IL)-1α, IL-1β, IL-1 α/β, and IL-1 receptor antagonist shows that IL-1β is crucial in turpentine-induced fever development and glucocorticoid secretion. *J. Exp. Med*. **187**, 1463–1475 (1998).
37. Lancaster, G. I. & Henstridge, D. C. Body composition and metabolic caging analysis in high fat fed mice. *J. Vis. Exp*. **135**, 57280 (2018).
38. Liao, Y., Smyth, G. K. & Shi, W. The Subread aligner: fast, accurate and scalable read mapping by seed-and-vote. *Nucleic Acids Res*. **41**, e108 (2013).
39. Liao, Y., Smyth, G. K. & Shi, W. featureCounts: an efficient general purpose program for assigning sequence reads to genomic features. *Bioinformatics* **30**, 923–930 (2014).
40. Law, C. W., Chen, Y., Shi, W. & Smyth, G. K. voom: Precision weights unlock linear model analysis tools for RNA-seq read counts. *Genome Biol*. **15**, R29 (2014).
41. Ritchie, M. E. et al. limma powers differential expression analyses for RNA-sequencing and microarray studies. *Nucleic Acids Res*. **43**, e47 (2015).
42. McCarthy, D. J. & Smyth, G. K. Testing significance relative to a fold-change threshold is a TREAT. *Bioinformatics* **25**, 765–771 (2009).
43. Buenrostro, J. D., Giresi, P. G., Zaba, L. C., Chang, H. Y. & Greenleaf, W. J. Transposition of native chromatin for fast and sensitive epigenomic profiling of open chromatin, DNA-binding proteins and nucleosome position. *Nat. Methods* **10**, 1213–1218 (2013).

Acknowledgements This work was funded by the National Health and Medical Research Council (NHMRC, project grants 1106378 and 1149062 and fellowship 1139607 to A.K.), the Sylvia and Charles Viertel Foundation (fellowship to A.K.), the Diabetes Australia (grant Y18G-VASA to A.V.) and grants from the US NIH (R01DK092541) and JPB Foundation (to D.M.). W.S. is funded by a Walter and Eliza Hall Institute Centenary Fellowship funded by a donation from CSL. M.A.F. is a senior Principal Research Fellow of the NHMRC. P.A.B. was funded by an NBCF Career Development Fellowship. R.G.S. is an American Diabetes Association Postdoctoral

fellow (1-17-PMF-005). J.D.Z. and R.A.D. are supported by funding from The Sir Edward Dunlop Medical Research Foundation, The Austin Health Research Foundation and a Les and Eva Erdi Research Grant. R.A.D. was funded by a fellowship from the Australian and New Zealand Bone and Mineral Society. We thank T. Korn for help with experiments, and G. Risbridger, K. S. Korach, M. Ernst, J. Silke and W. C. Boon for mice.

Author contributions A.V. and A.K. designed the experiments, interpreted the results and wrote the paper. A.V. performed most of the experiments. D.C., Y.L. and W.S. analysed the sequencing data. J.B. and P.A.B. performed stromal cell analyses. R.G. and T.S. contributed to RNA-seq and ATAC-seq experiments. C.L., R.G.S. and D.M. performed adoptive transfer experiments using VAT TCR Tg mice as well as intracellular staining and flowcytometric analyses of IL-33 protein expression. S.L. and S.V.T. performed flow cytometry analyses. Y.Z. contributed to experiments using CCR2-deficient mice. S.L.N., J.D.Z., R.A.D. and P.A.B. contributed mice and scientific discussion. K.B. performed ICI 182-780 treatment and contributed to the hormone supplementation experiments. E.C. and N.T. performed the COX-inhibitor experiments. D.C.H. and M.A.F. did metabolic experiments, and T.G. and N.C. performed the parabiosis experiments.

Competing interests The authors declare no competing interests.

Additional information

Supplementary information is available for this paper at https://doi.org/10.1038/s41586-020-2040-3.

Correspondence and requests for materials should be addressed to A.V. or A.K.

Peer review information *Nature* thanks Alexander Chervonsky, Shigeo Koyasu and the other, anonymous, reviewer(s) for their contribution to the peer review of this work.

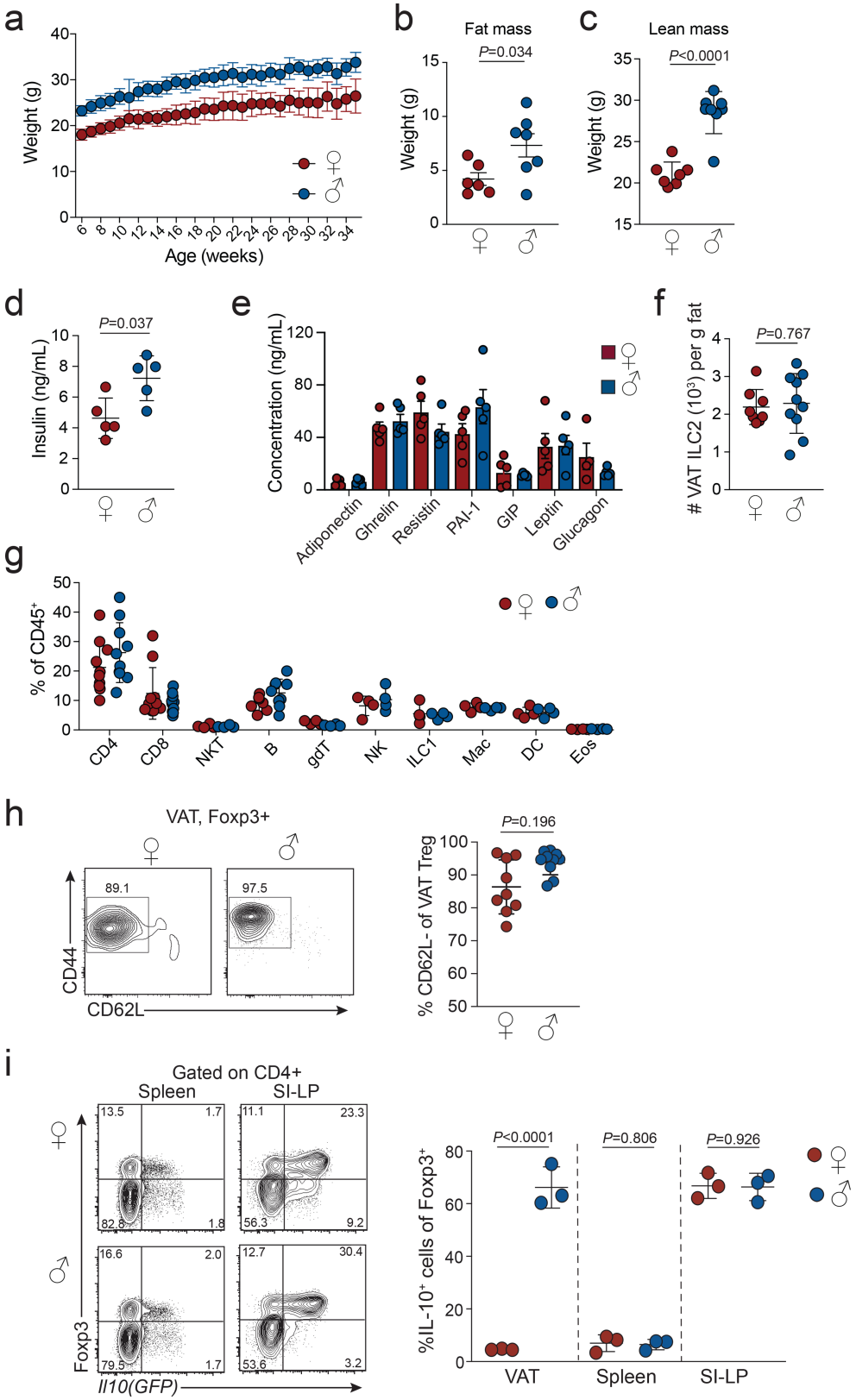

Extended Data Fig. 1 | See next page for caption.

Extended Data Fig. 1 | Multiple physiological and cellular parameters differ between male and female mice. a, Weight gain of normal chow diet fed wild-type male and female mice with age ($n = 6$ mice of each sex). **b**–**e**, Multiple physiological parameters measured in age matched wild-type male and female mice, including fat mass ($n = 7$ mice of each sex) (**b**), lean mass ($n = 7$ mice of each sex) (**c**), serum insulin levels ($n = 5$ mice of each sex) (**d**) and serum adipokine levels 6 h post fasting ($n = 5$ mice of each sex) (**e**). **f**, Numbers of ILC2s in male and female VAT from 12–15-week-old mice. $n = 8$ females, $n = 10$ males. **g**, Proportions of different VAT resident immune cells determined from male and female mice ($n = 4$–9). **h**, Expression of CD44 and CD62L in VAT T_{reg} cells from male and female wild-type mice. Graph on the right shows quantification ($n = 9$ mice of each sex). **i**, Flow cytometry plots (left) showing *Foxp3* (RFP) and *Il10* (GFP) expression in spleens and small intestine lamina propria (SI-LP) and quantification (right) of *Il10* $(GFP)^+$ T_{reg} cells in VAT, spleen and SI-LP resident $CD4^+$ T cells of female and male *Foxp3*^{RFP}*Il10*^{GFP} double-reporter mice ($n = 3$ mice of each sex). Unpaired *t*-test was performed (two-tailed). Data are mean ± s.d. Data pooled or representative of two independent experiments.

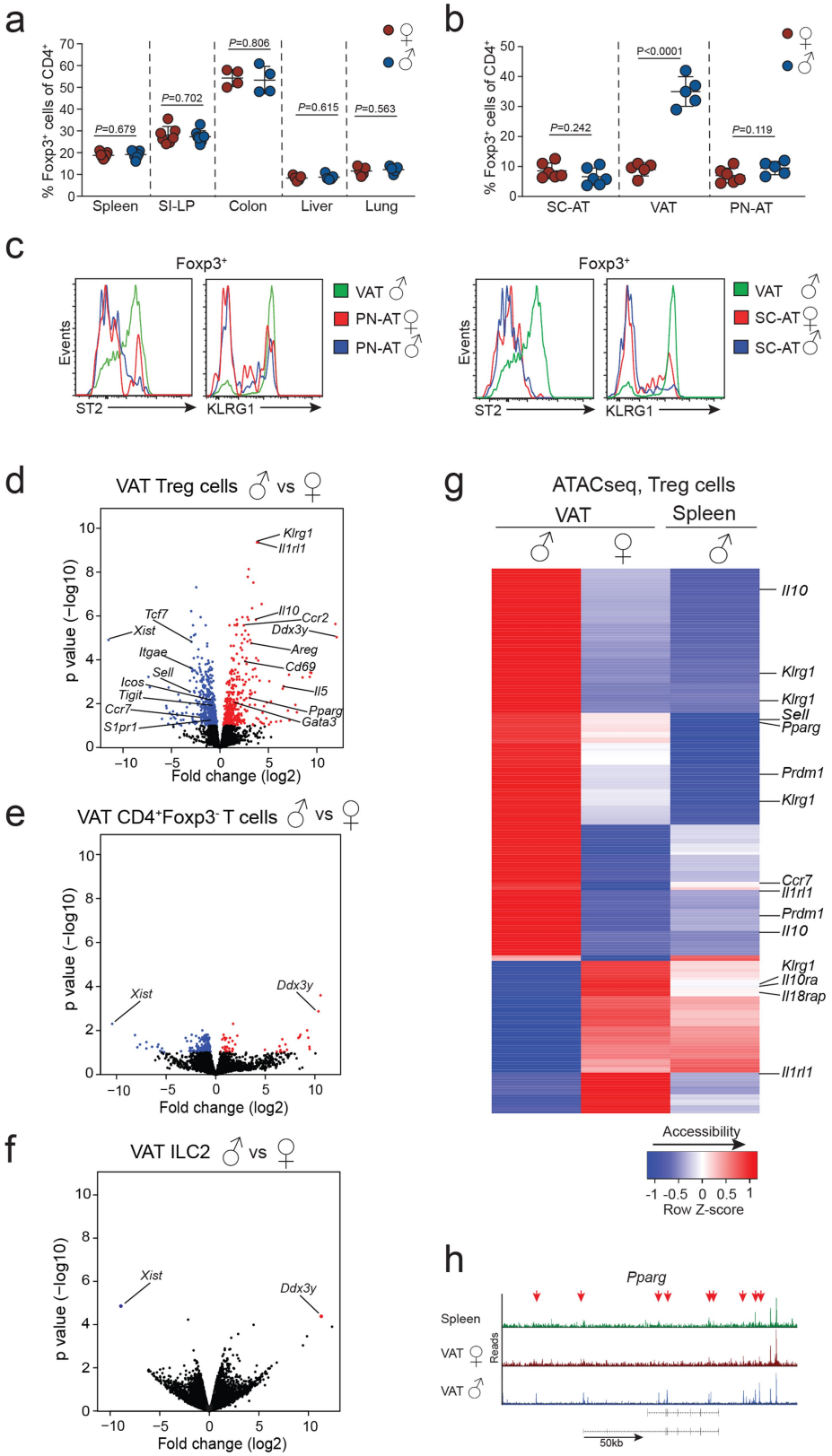

Extended Data Fig. 2 | See next page for caption.

Extended Data Fig. 2 | VAT-specific sexual dimorphism in T_{reg} cells is underpinned by unique transcriptional signatures and chromatin accessibility. a, Percentages of $FOXP3^+$ cells in spleens ($n = 6$ of each sex), small intestine lamina propria (SI-LP) ($n = 7$, females and males), colons ($n = 4$ of each sex), livers and lungs ($n = 5$ of each sex) from 25–30-week-old wild-type mice. **b**, Percentages of $FOXP3^+$ cells in subcutaneous adipose tissue (SC-AT) ($n = 6$ of each sex), VAT ($n = 5$ of each sex) and perinephric adipose tissue (PN-AT) ($n = 6$ of each sex) from 25–30-week-old wild-type mice. **c**, Expression of ST2 and KLRG1 in T_{reg} cells from the PN-AT (left) and SC-AT (right) of wild-type male and female mice. T_{reg} cells from male VAT are shown in green as positive control. **d**–**f**, Volcano plots show genes differentially expressed between male and female VAT T_{reg} cells (**d**), VAT $CD4^+FOXP3^-$ T cells (**e**) and VAT-ILC2s (**f**). Each dot represents a gene. Differentially expressed genes are marked in blue (downregulated) or red (upregulated). **g**, Heat map shows chromatin accessibility of VAT T_{reg}-signature genes assessed by ATAC-seq. Data displayed from male VAT T_{reg} cells, female VAT T_{reg} cells and male splenic T_{reg} cells. **h**, ATAC-seq tracks show chromatin accessibility at the *Pparg* locus of male splenic T_{reg} cells (green) and T_{reg} cells from female (red) and male (blue) VAT. Arrows indicate regions of differential chromatin accessibility. Data in **a**, **b** are pooled or representative of two independent experiments; two-tailed unpaired *t*-test. Data are mean ± s.d. Sequencing experiments performed in duplicates. For each RNA-seq sample, VAT T_{reg} cells were sorted from male ($n = 5$) and female ($n = 12$) $Foxp3^{RFP}$ mice. For ATAC-seq, each sample contained T_{reg} cells from $n = 4$ males and $n = 10$ females. Experiments were performed with 25–32-week-old mice. Statistical methods and software packages for sequencing data are described in Methods.

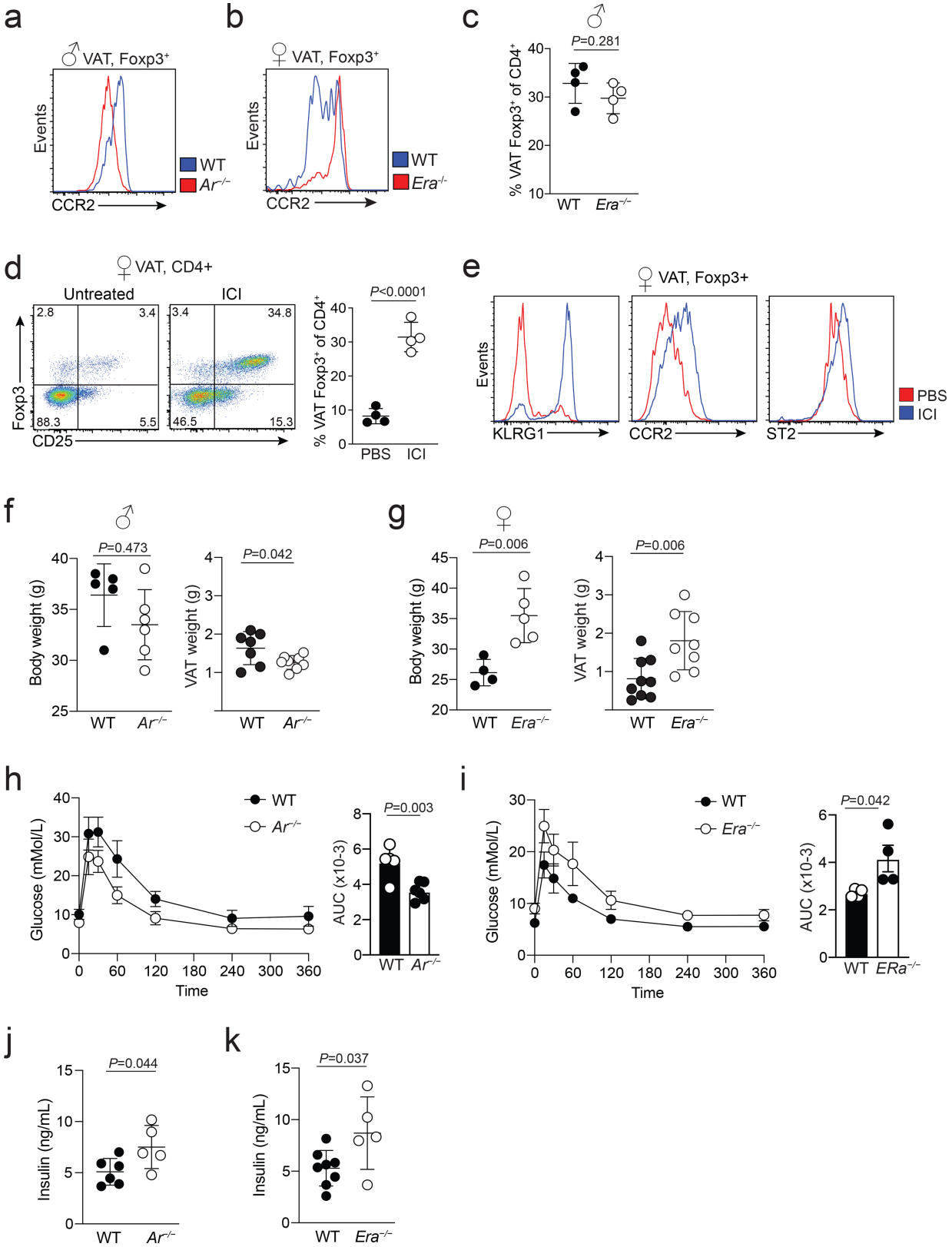

Extended Data Fig. 3 | See next page for caption.

Extended Data Fig. 3 | Opposing functions of male and female sex hormones in regulating VAT inflammation, T_{reg} cell recruitment and glucose tolerance. **a**, **b**, Representative flow cytometry histograms showing expression of CCR2 in wild-type and $Ar^{-/-}$ VAT T_{reg} cells (**a**) and wild-type and $Era^{-/-}$ VAT T_{reg} cells (**b**). **c**, Frequency of VAT T_{reg} cells in male wild-type and $Era^{-/-}$ mice ($n = 4$ of each genotype). **d**, Flow cytometry plots (left) show VAT T_{reg} cells from control and ICI182-780-treated female mice; graph (right) shows quantification ($n = 4$ for both conditions). **e**, Expression of indicated markers in control and ICI 182-780-treated female VAT T_{reg} cells. **f**, Body mass (left) ($n = 5$ wild type; $n = 6$ $Ar^{-/-}$) and VAT mass (right) ($n = 7$ wild type; $n = 8$ $Ar^{-/-}$) from 20–25-week-old male wild-type and $Ar^{-/-}$ mice. **g**, Body mass (left) ($n = 4$ wild type; $n = 5$ $Era^{-/-}$) and VAT mass (right) ($n = 9$ wild type; $n = 8$ $Era^{-/-}$) from 20–25-week-old female WT and $Era^{-/-}$ mice. **h**, **i**, Oral glucose-tolerance test (left) and area under the curve (right) comparing age-matched male wild-type and $Ar^{-/-}$ mice ($n = 4$ wild type; $n = 5$ $Ar^{-/-}$) (**h**), or female wild-type and $Era^{-/-}$ mice ($n = 4$, wild type and $Era^{-/-}$ of each genotype) (**i**). **j**, **k**, Fasting serum insulin levels in wild-type ($n = 6$) and $Ar^{-/-}$ ($n = 5$) male mice (**j**), and in WT ($n = 8$) and $Era^{-/-}$ ($n = 5$) female mice (**k**). Two-tailed unpaired *t*-test; data are mean ± s.d. Data are pooled or representative of two independent experiments.

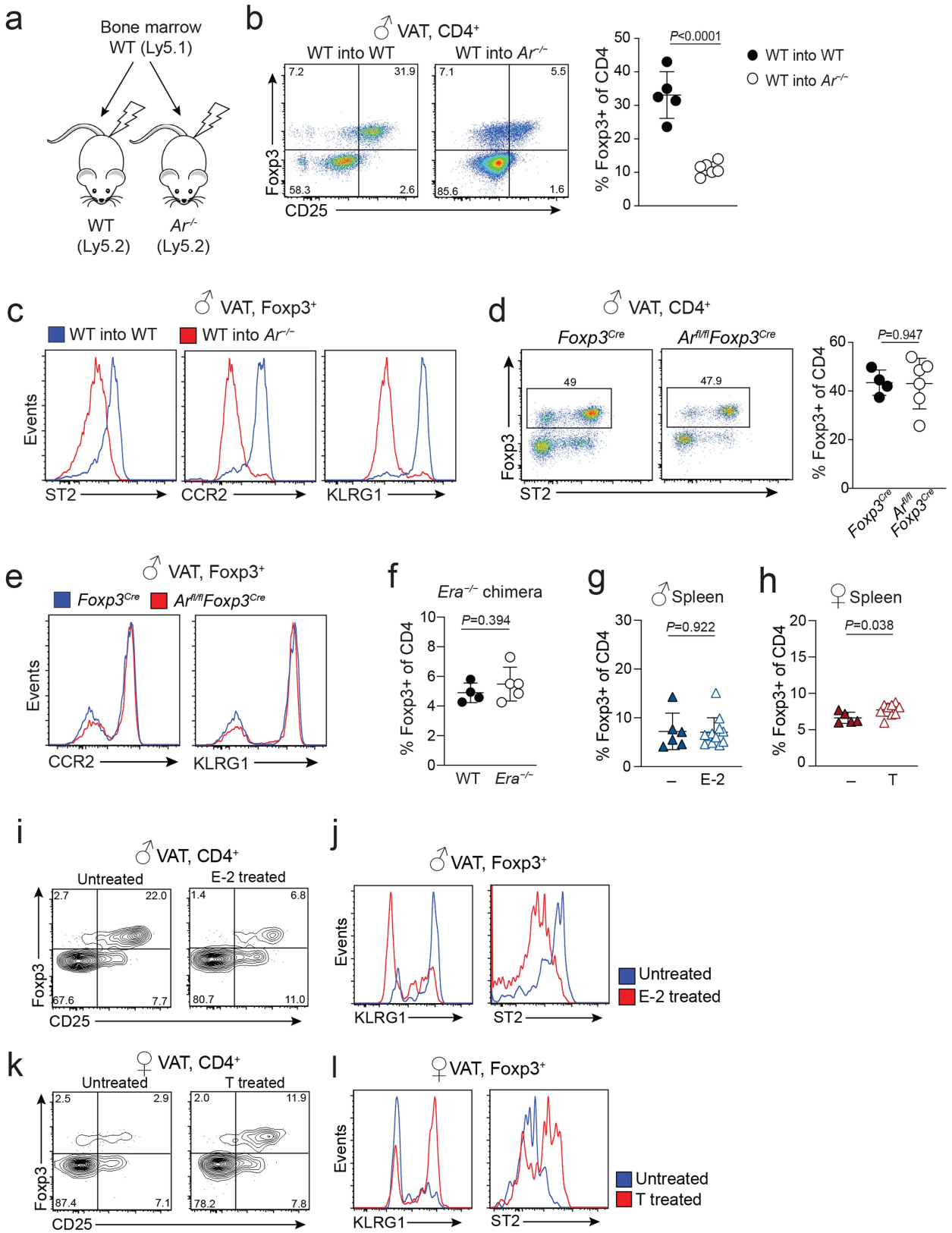

Extended Data Fig. 4 | See next page for caption.

Extended Data Fig. 4 | VAT T_{reg} cell extrinsic function of sex hormones. **a**, Schematic shows the strategy used to make bone marrow chimeric mice using wild-type and $Ar^{-/-}$ recipients. **b**, Proportions of T_{reg} cells from the VAT of irradiated wild-type ($n = 5$) and $Ar^{-/-}$ ($n = 6$) mice that received wild-type bone marrow. Quantification on the right. **c**, Expression of indicated cell surface markers on VAT T_{reg} cells from wild-type and $Ar^{-/-}$ mice that were reconstituted with wild-type bone marrow (from **b**). **d**, Flow cytometry plots (left) show expression of FOXP3 and ST2 in VAT $CD4^+$ T cells from male $Ar^{fl/fl}Foxp3^{cre}$ ($n = 6$) and $Foxp3^{cre}$ ($n = 4$) control mice. Quantification on the right. **e**, Expression of CCR2 and KLRG1 in VAT T_{reg} cells from $Ar^{fl/fl}Foxp3^{cre}$ and control mice (from **d**). **f**, Percentages of wild-type and $Era^{-/-}$ T_{reg} cells in the VAT of female bone marrow chimeric mice. Irradiated wild-type female Ly5.1 recipient mice were reconstituted with a mixture of female Ly5.2 wild-type ($n = 4$) and female $Era^{-/-}$ ($n = 5$) bone marrow cells. **g**, **h**, Percentages of splenic T_{reg} cells in oestrogen-treated ($n = 12$) and untreated ($n = 6$) male wild-type mice (**g**) and in testosterone-treated ($n = 9$) and untreated ($n = 5$) female wild-type mice (**h**). **i**, Expression of FOXP3 and CD25 in VAT $CD4^+$ T cells isolated from oestrogen-treated or untreated male wild-type mice. **j**, Flow cytometry histograms show expression of KLRG1 and ST2 in VAT T_{reg} cells from oestrogen-treated or untreated male wild-type mice. **k**, Expression of FOXP3 and CD25 in VAT CD4+ T cells isolated from testosterone-treated or untreated female wild-type mice. **l**, Expression of KLRG1 and ST2 in VAT T_{reg} cells from testosterone-treated or untreated female wild-type mice. Two-tailed unpaired *t*-test. Data are mean ± s.d. Data are pooled or representative of two independent experiments.

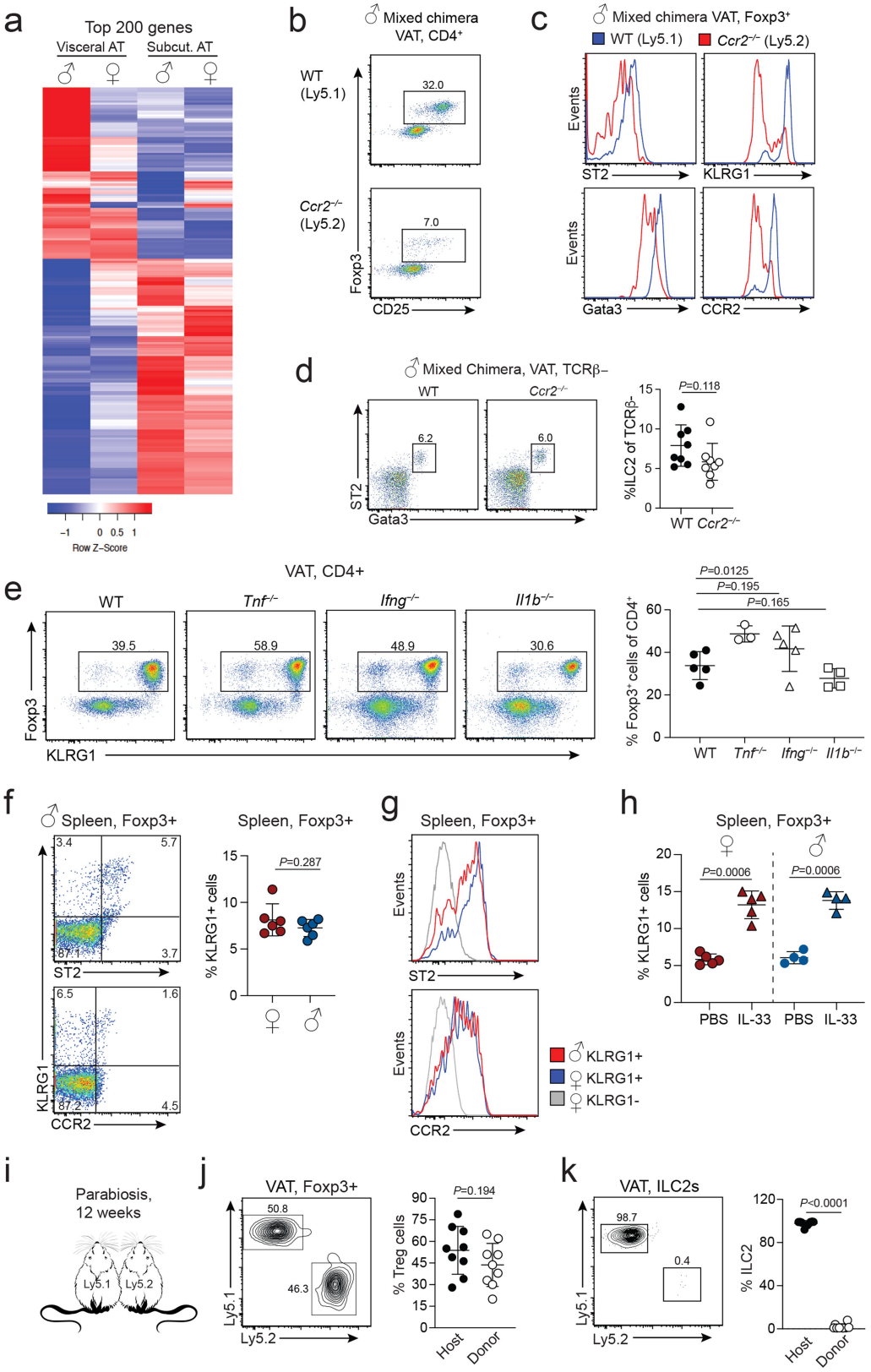

Extended Data Fig. 5 | See next page for caption.

Extended Data Fig. 5 | Sex-specific VAT inflammation, T_{reg} cell recruitment and maintenance in VAT. a, Heat map shows top-200 differentially expressed genes between male and female VAT and subcutaneous adipose tissue (SC-AT). Duplicate samples used for RNA-seq. For each sample, VAT or SC-AT from three mice was pooled for RNA extraction. **b**, Proportions of T_{reg} cells in wild-type and *Ccr2*$^{-/-}$ compartments of mixed bone marrow chimeric mice. **c**, Expression of specified markers in wild-type and *Ccr2*$^{-/-}$ VAT T_{reg} cells from male mixed bone marrow chimeric mice. **d**, Flow cytometry plots (left) and quantification (right) of wild-type and CCR2-deficient ILC2s in the VAT of male chimeric mice containing congenically marked wild-type ($n = 8$) and *Ccr2*$^{-/-}$ ($n = 8$) haematopoietic cells. **e**, Expression of FOXP3 and KLRG1 in wild-type ($n = 5$), *Tnf*$^{-/-}$ ($n = 3$), *Ifng*$^{-/-}$ ($n = 5$) and *Il1b*$^{-/-}$ ($n = 4$) mice. Graph on the right shows quantification. **f**, Expression of KLRG1 and ST2 (top) and KLRG1 and CCR2 (bottom) in splenic T_{reg} cells from wild-type male mice. Graph (right) shows percentages of KLRG1$^+$ cells of T_{reg} cells in the spleen of wild-type male and female mice ($n = 6$ of each sex). **g**, ST2 and CCR2 expression in male and female KLRG1$^+$ splenic T_{reg} cells. **h**, Graph shows percentages of KLRG1$^+$ cells of T_{reg} cells in the spleens of female ($n = 5$) and male ($n = 4$) mice treated with PBS or IL-33. **i**, Schematic of parabiosis experiment. **j**, **k**, Flow cytometry plots (left) and quantification (right) show proportions of T_{reg} cells ($n = 9$) (**j**) and ILC2s ($n = 9$) (**k**) in the VAT of parabiotic wild-type female mice that were paired for 12 weeks. Two-tailed unpaired *t*-test. Data are mean ± s.d. Data are pooled or representative of two independent experiments.

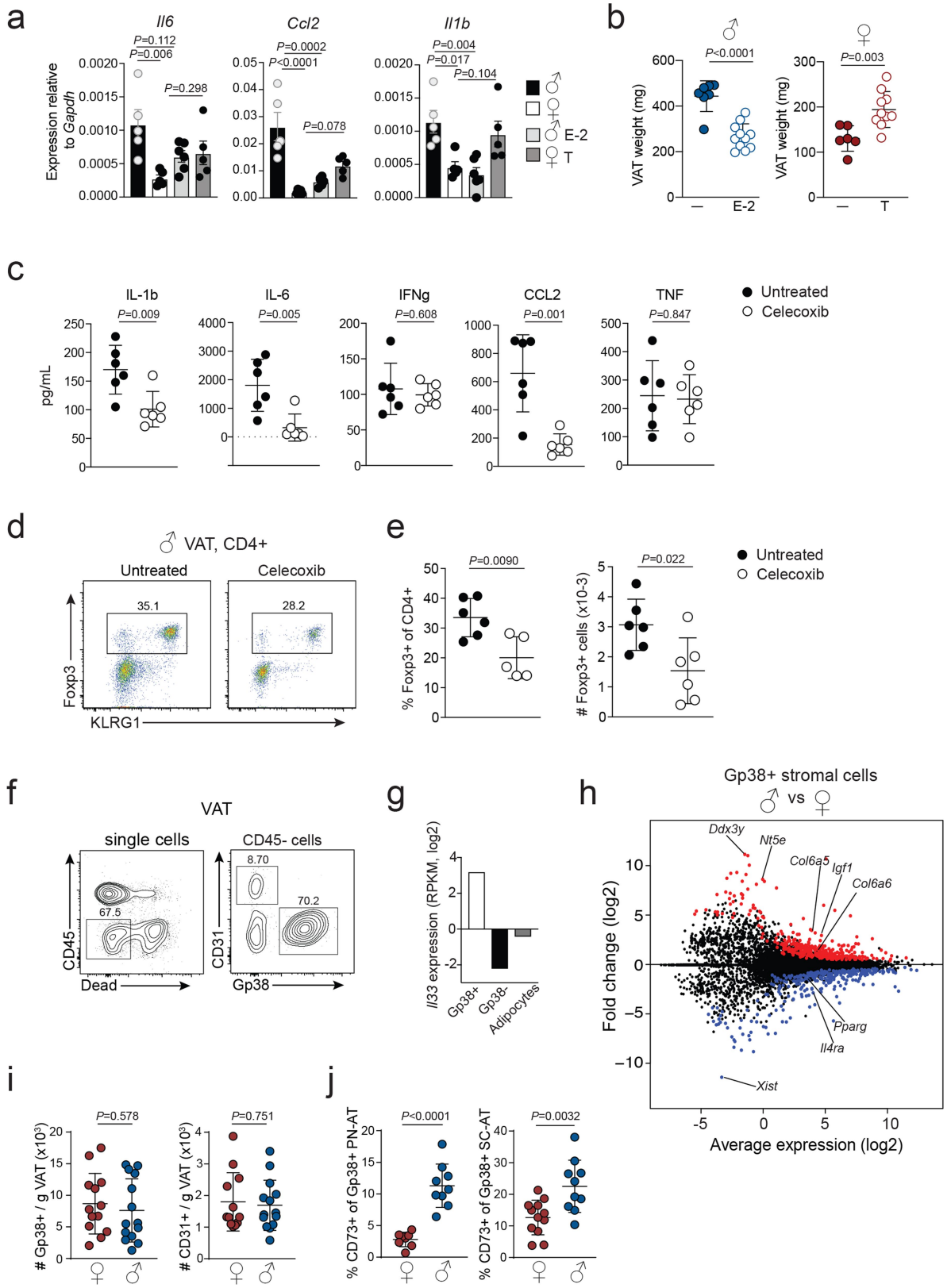

Extended Data Fig. 6 | See next page for caption.

Extended Data Fig. 6 | Sex-hormonal control of VAT inflammation and stromal cell differentiation. a, Expression of indicated genes in the VAT of testosterone- or oestrogen-treated male and female wild-type mice measured by quantitative PCR. Untreated females and males, testosterone-treated females ($n = 5$); oestrogen-treated males ($n = 6$). **b**, VAT weight from untreated ($n = 7$) and oestrogen-treated ($n = 11$) wild-type male (left) and untreated ($n = 6$) and testosterone-treated ($n = 10$) wild-type female (right) mice. **c**, Concentrations of indicated proinflammatory cytokines in the mesenteric lymph nodes of celecoxib-treated or untreated wild-type male mice ($n = 6$ per condition) measured by cytokine bead array. **d**, Expression of FOXP3 and KLRG1 in $CD4^+$ T cells isolated from the VAT of celecoxib-treated and untreated male wild-type mice. **e**, Percentages (left) and numbers (right) of $FOXP3^+$ T_{reg} cells in the VAT of celecoxib-treated and untreated wild-type male mice ($n = 6$ per condition). **f**, Gating strategy used to identify VAT $CD31^+$ endothelial cells and $Gp38^+$ stromal cells in the CD45- non-haematopoietic cell compartment of wild-type male and female mice. **g**, *Il33* transcript levels in $Gp38^+$ stromal and $Gp38^-CD31^+$ endothelial cells and in adipocytes from 25-week-old male mice (data from RNA-seq analysis, two samples per cell type). **h**, MA plot showing genes differentially expressed between male and female $Gp38^+$ VAT stromal cells. RNA-seq performed in duplicate samples. For each sample, the respective VAT stromal cell population was sorted from wild-type male ($n = 5$) and female ($n = 7$) mice. **i**, Numbers of $Gp38^+$ cells in female ($n = 13$) and male ($n = 14$) VAT (left) and $CD31^+$ cells (right) in female ($n = 11$) and male ($n = 14$) VAT from 25-week-old mice. **j**, Proportions of $CD73^+$ cells within the female ($n = 8$) and male ($n = 9$) $Gp38^+$ stromal compartment of perinephric adipose tissue (PN-AT, left) and subcutaneous adipose tissue (right) ($n = 12$ females; $n = 10$ males). In **a**, one-way ANOVA was performed. Other data were analysed using two-tailed unpaired *t*-test. Data are mean ± s.d., except in **a**, where data are mean ± s.e.m. Data are pooled or representative of two independent experiments.

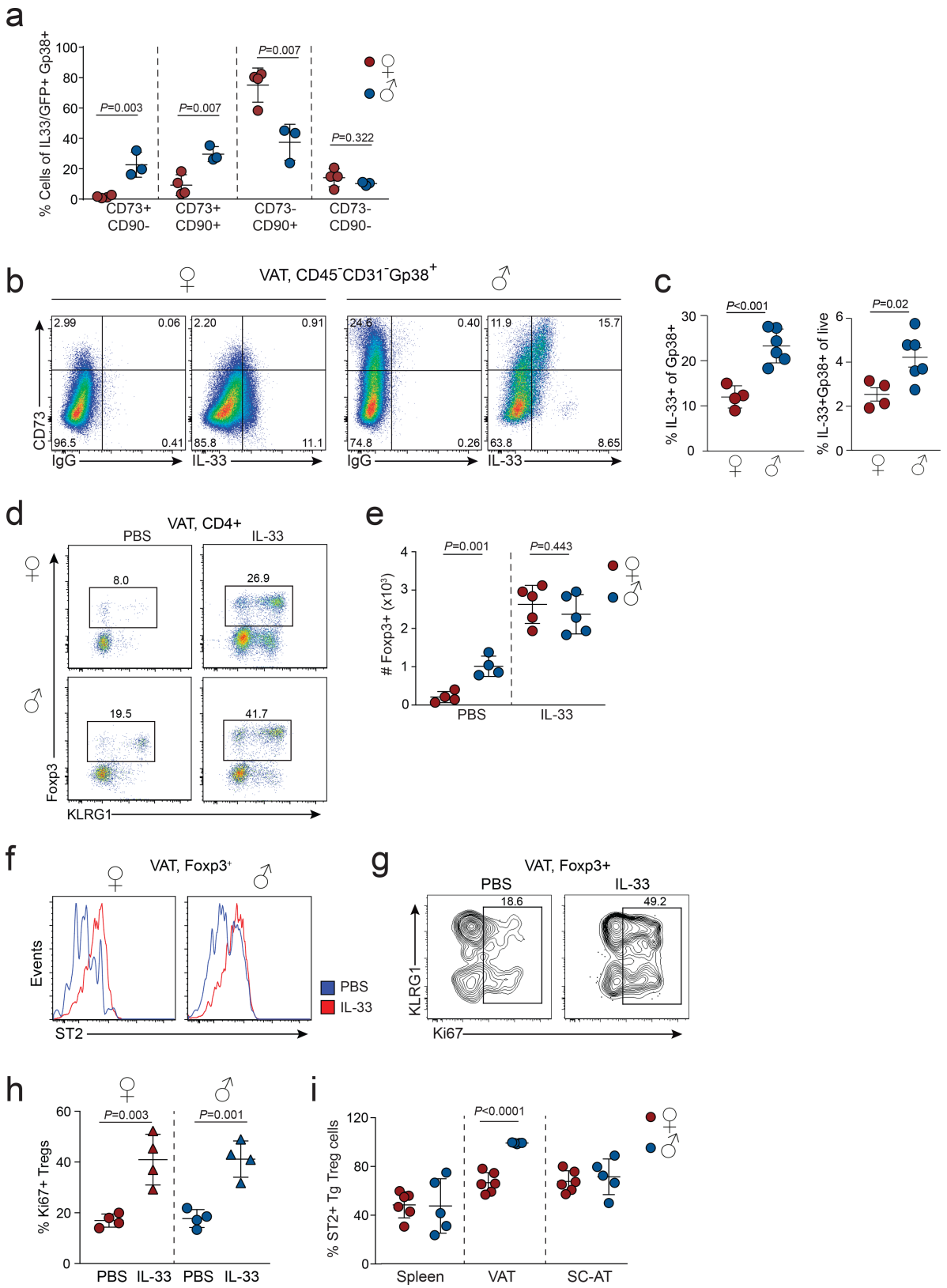

Extended Data Fig. 7 | See next page for caption.

Extended Data Fig. 7 | Sex-specific distribution of IL-33$^+$ VAT stromal cells and VAT T_{reg} cell response to IL-33 administration. a, Percentages of IL-33$^+$ cells within each VAT Gp38$^+$ stromal cell compartment of female ($n = 4$) and male ($n = 3$) *Il33*^{GFP} mice. **b**, IL-33 expression in CD45$^-$CD31$^-$Gp38$^+$ stromal cells of wild-type mice as measured by intracellular staining. IgG was used as a control. **c**, Percentage of IL-33$^+$ cells in the VAT Gp38$^+$ stromal cell compartment of wild-type female ($n = 4$) and male ($n = 6$) mice (left) and percentages of IL-33$^+$Gp38$^+$ of live cells in VAT (right). **d**–**h**, IL-33 ($n = 5$) or PBS (mock) ($n = 4$) was administered to 12-week-old male and female wild-type mice. Expression of FOXP3 and KLRG1 in VAT CD4$^+$ T cells (**d**), numbers of VAT T_{reg} cells (**e**), ST2 expression in VAT T_{reg} cells from IL-33- or PBS-treated (**f**), expression of KLRG1 and Ki67 in VAT T_{reg} cells of male mice (**g**) and quantification of Ki67$^+$ VAT T_{reg} cells in female and male wild-type mice ($n = 4$ of each sex) (**h**). **i**, T_{reg} cells were sorted from the spleens of transgenic mice expressing a VAT-specific T cell receptor[25] and transferred into congenically marked female ($n = 6$) or male ($n = 5$) wild-type mice. Percentages of ST2$^+$ TCR transgenic (Tg) T_{reg} cells within the adipose tissue 12 weeks after adoptive transfer. Two-tailed unpaired *t*-test. Data are mean ± s.d. Data are pooled or representative of two independent experiments.

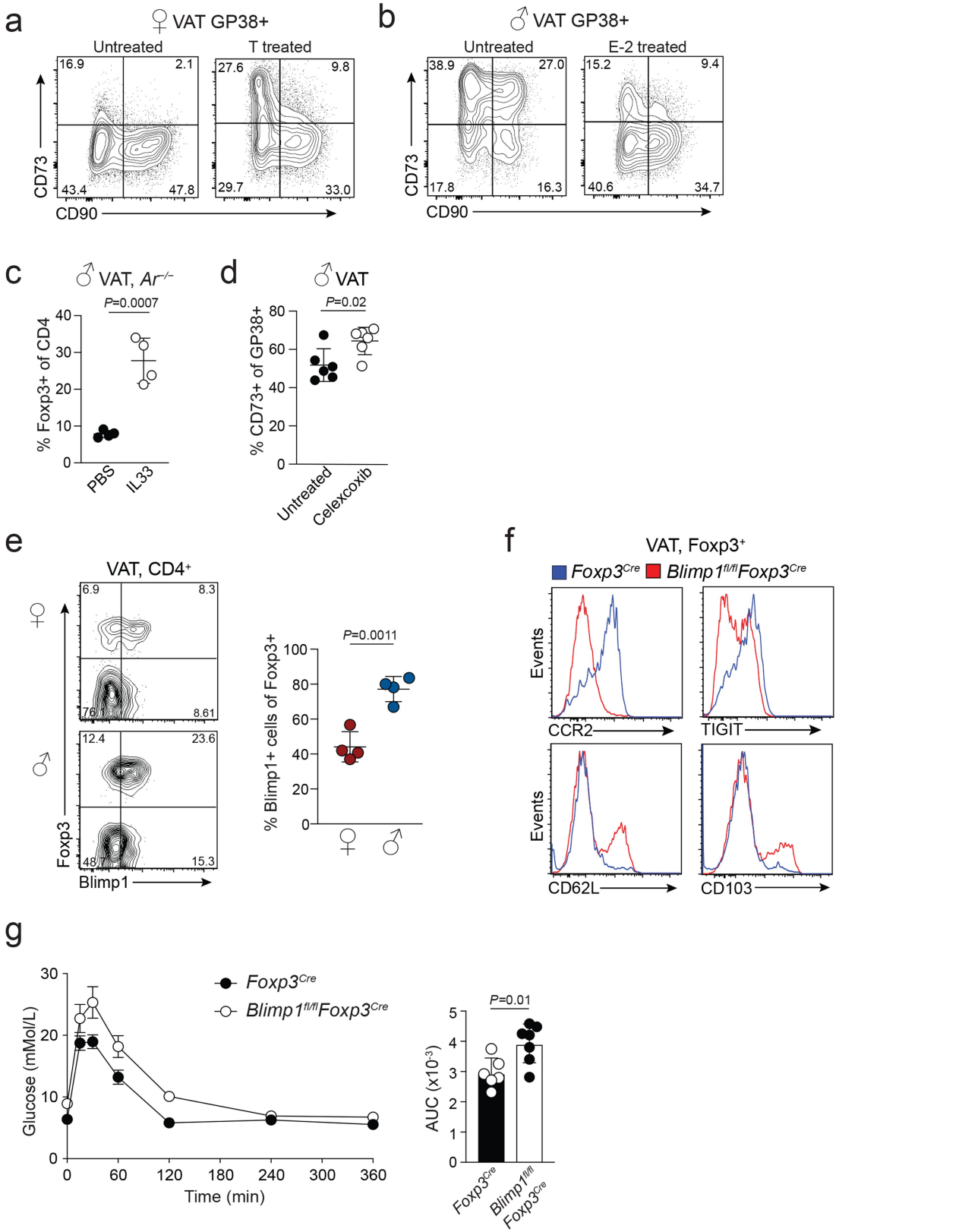

Extended Data Fig. 8 | Sex-hormonal regulation of CD73$^+$ VAT stromal cell differentiation and BLIMP1 regulation of VAT T_{reg} cells and organismal metabolism. a, Flow cytometry plots from testosterone-treated and untreated female wild-type mice showing expression of CD73 and CD90 in Gp38$^+$ VAT stromal cells. **b**, Flow cytometry plots from oestrogen-treated and untreated male wild-type mice showing expression of CD73 and CD90 in Gp38$^+$ VAT stromal cells. **c**, Percentages of VAT T_{reg} cells in male *Ar*$^{-/-}$ mice treated with PBS ($n = 4$) or IL-33 ($n = 4$). **d**, Percentages of CD73$^+$ stromal cells in celecoxib-treated ($n = 6$) or untreated ($n = 5$) male mice. **e**, Expression of *Foxp3* (RFP) and *Blimp1* (GFP) in male and female VAT T_{reg} cells from *Foxp3*^{RFP}*Blimp1*^{GFP} double-reporter mice ($n = 4$ of each sex). Percentages of *Blimp1* (GFP)$^+$ cells among *Foxp3* (RFP)$^+$ T_{reg} cells. **f**, Expression of indicated molecules in *Foxp3*^{cre} and *Blimp1*$^{fl/fl}$*Foxp3*^{cre} VAT T_{reg} cells. **g**, Oral glucose-tolerance test in normal chow diet-fed 25-week-old male *Blimp1*$^{fl/fl}$*Foxp3*^{cre} ($n = 7$) and *Foxp3*^{cre} ($n = 6$) mice. Graph on the right shows AUC. Two-tailed unpaired *t*-test. Data are mean ± s.d. Data are pooled or representative of two independent experiments.

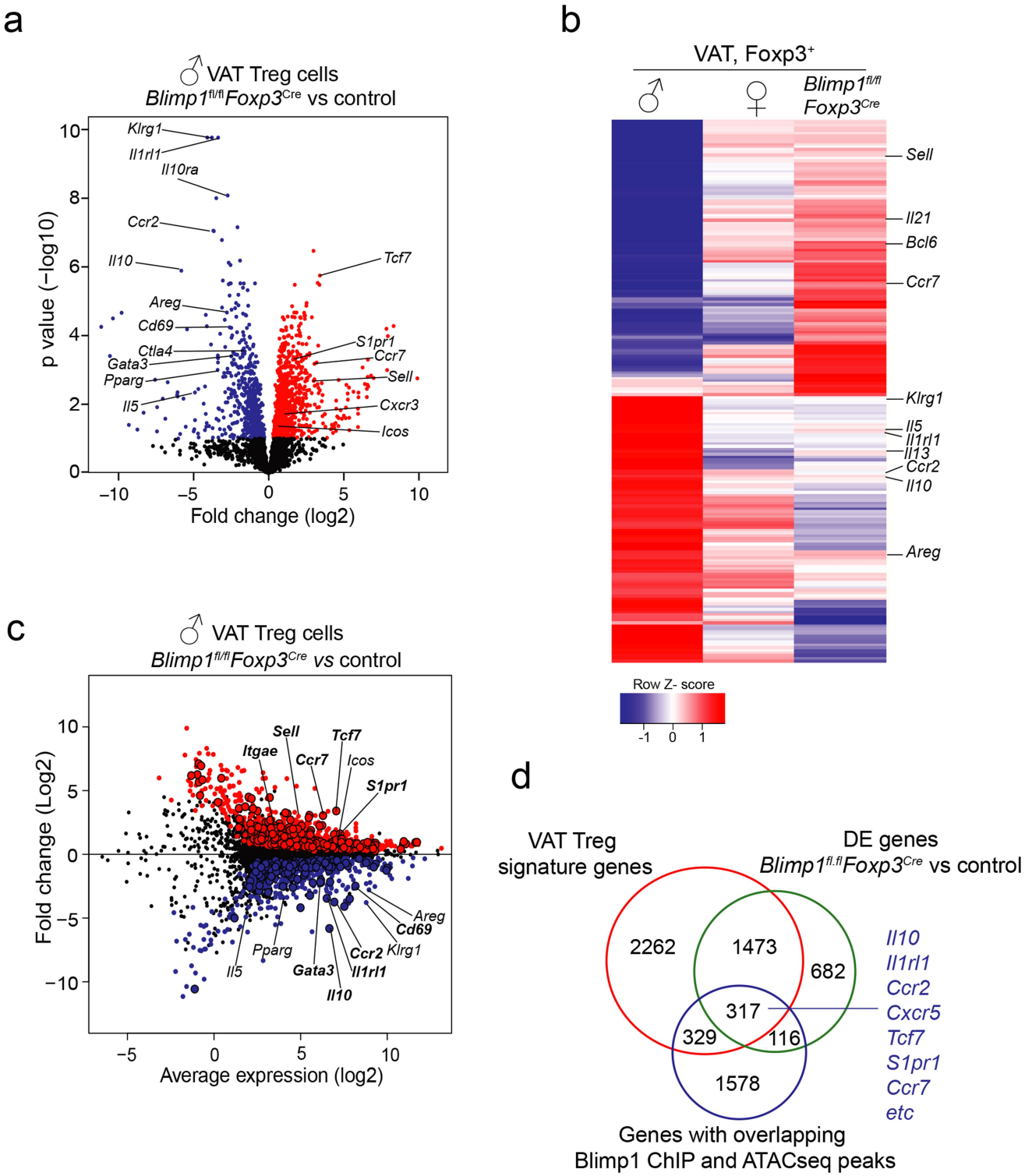

Extended Data Fig. 9 | BLIMP1 establishes the VAT T_{reg} cell transcriptional and chromatin landscapes. a, Volcano plot shows genes differentially expressed between male *Blimp1*$^{fl/fl}$*Foxp3*^{cre} and control VAT T_{reg} cells. For each genotype, duplicate samples were used for RNA-seq. Each sample contains VAT T_{reg} cells from $n = 7$ *Blimp1*$^{fl/fl}$*Foxp3*^{cre} and $n = 5$ *Foxp3*^{cre} mice. **b**, Heat map shows top-200 genes differentially expressed between wild-type male and female VAT T_{reg} cells and *Blimp1*$^{fl/fl}$*Foxp3*^{cre} male VAT T_{reg} cells. **c**, MD plot shows expression of genes in *Blimp1*$^{fl/fl}$*Foxp3*^{cre} and *Foxp3*^{cre} VAT T_{reg} cells. Each dot represents a gene; genes highlighted in red are up regulated, and in blue are downregulated, in *Blimp1*$^{fl/fl}$*Foxp3*^{cre} VAT T_{reg} cells. Larger dots with black outline indicate genes that are also bound by BLIMP1 in regions of open chromatin in VAT T_{reg} cells. **d**, Venn diagram shows overlap between genes differentially expressed between male VAT T_{reg} cells and male splenic T_{reg} cells (VAT T_{reg} cell signature), male *Blimp1*$^{fl/fl}$*Foxp3*^{cre} and control VAT T_{reg} cells and genes that show BLIMP1 ChIP binding in regions of open chromatin (peaks) of male VAT T_{reg} cells. Statistical methods and software packages described in Methods.

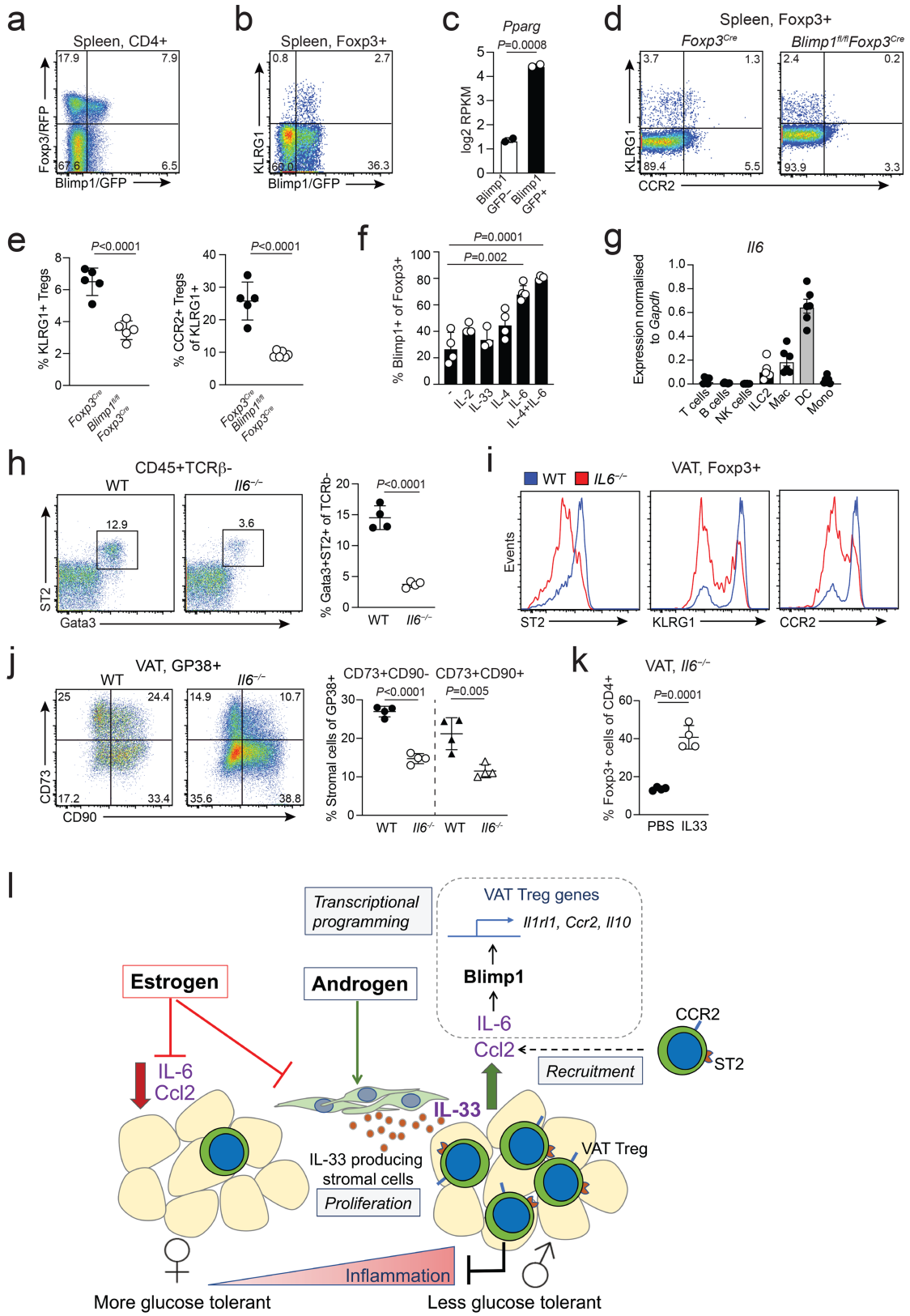

Extended Data Fig. 10 | See next page for caption.

Extended Data Fig. 10 | Blimp1 regulates putative VAT T_{reg} cell precursors, diverse functions of IL-6 in the VAT, and a model of the sex-hormone-mediated circuitry that mediates recruitment, expansion and function of VAT T_{reg} cells. a, Expression of *Foxp3* (RFP) and *Blimp1* (GFP) in splenic $CD4^+$ T cells from $Foxp3^{RFP}Blimp1^{GFP}$ mice. **b**, Expression of *Blimp1* (GFP) and KLRG1 in splenic T_{reg} cells. **c**, *Pparg* expression in *Blimp1* $(GFP)^+$ versus *Blimp1* $(GFP)^-$ splenic T_{reg} cells. Bar graph generated from RNA-seq read counts[26]. **d**, Expression of KLRG1 and CCR2 in splenic T_{reg} cells from $Foxp3^{cre}$ and $Blimp1^{fl/fl}Foxp3^{cre}$ mice. **e**, Graphs on the right show percentages of $KLRG1^+$ cells among splenic T_{reg} cells of $Foxp3^{cre}$ ($n = 5$) and $Blimp1^{fl/fl}Foxp3^{cre}$ ($n = 6$) mice and percentages of $CCR2^+$ cells within the $KLRG1^+$ fraction of splenic T_{reg} cells. **f**, Proportion of *Blimp1* $(GFP)^+$ T_{reg} cells obtained after *Blimp1* $(GFP)^-$ T_{reg} cells were sorted from $Foxp3^{RFP}Blimp1^{GFP}$ mice and cultured in the presence of indicated cytokines ($n = 3$–4). **g**, Expression of *Il6* transcripts as measured by quantitative PCR in haematopoietic cell populations sorted from the male VAT ($n = 6$). **h**, Flow cytometry plots (left) and quantification (right) of ILC2s in the VAT of male wild-type and $Il6^{-/-}$ ($n = 4$ per genotype) mice. **i**, Flow cytometry histograms show expression of indicated markers in wild-type and $Il6^{-/-}$ VAT T_{reg} cells. **j**, Expression of CD73 and CD90 in wild-type and $Il6^{-/-}$ ($n = 4$ per genotype) VAT $Gp38^+$ cells (left). Percentages of $CD73^+CD90^-$ and $CD73^+CD90^+$ stromal cells in the VAT of male wild-type and $Il6^{-/-}$ ($n = 4$ per genotype) mice (right). **k**, Percentages of VAT T_{reg} cells in male $Il6^{-/-}$ mice treated with PBS or IL-33. Two-tailed unpaired *t*-test. Data are mean ± s.d. Data pooled or representative of two independent experiments. **l**, Model of the sex-hormone-mediated circuitry that mediates recruitment, expansion and function of VAT T_{reg} cells. T_{reg} cells are recruited to the VAT in a CCL2–CCR2-dependent manner. IL-6 induces the expression of transcription factor BLIMP1, which in turn activates expression of prototypical VAT T_{reg} signature genes IL-33 receptor ST2, CCR2 and IL-10. IL-33 production by androgen-responsive stromal cells leads to local expansion of VAT T_{reg} cells in the male VAT, which in turn mediate repression of VAT inflammation.

nature research

Corresponding author(s): 2018-09-13125C

Last updated by author(s): 2019/12/17

Reporting Summary

Nature Research wishes to improve the reproducibility of the work that we publish. This form provides structure for consistency and transparency in reporting. For further information on Nature Research policies, see Authors & Referees and the Editorial Policy Checklist.

Statistics

For all statistical analyses, confirm that the following items are present in the figure legend, table legend, main text, or Methods section.

n/a	Confirmed	
☐	☒	The exact sample size (*n*) for each experimental group/condition, given as a discrete number and unit of measurement
☐	☒	A statement on whether measurements were taken from distinct samples or whether the same sample was measured repeatedly
☐	☒	The statistical test(s) used AND whether they are one- or two-sided *Only common tests should be described solely by name; describe more complex techniques in the Methods section.*
☒	☐	A description of all covariates tested
☒	☐	A description of any assumptions or corrections, such as tests of normality and adjustment for multiple comparisons
☐	☒	A full description of the statistical parameters including central tendency (e.g. means) or other basic estimates (e.g. regression coefficient) AND variation (e.g. standard deviation) or associated estimates of uncertainty (e.g. confidence intervals)
☐	☒	For null hypothesis testing, the test statistic (e.g. *F*, *t*, *r*) with confidence intervals, effect sizes, degrees of freedom and *P* value noted *Give P values as exact values whenever suitable.*
☒	☐	For Bayesian analysis, information on the choice of priors and Markov chain Monte Carlo settings
☒	☐	For hierarchical and complex designs, identification of the appropriate level for tests and full reporting of outcomes
☒	☐	Estimates of effect sizes (e.g. Cohen's *d*, Pearson's *r*), indicating how they were calculated

Our web collection on statistics for biologists contains articles on many of the points above.

Software and code

Policy information about availability of computer code

Data collection	Flow cytometry data was acquired using BD LSR Fortessa X20 (Diva software). RNA and ChIPseq data were generated using Illumina. Hand held Accu-chek Performa (Roche) glucometers were used to analyze blood glucose levels in GTT experiments. Promethion system (Sable Systems, Las Vegas, NV, USA) was used to collect metabolic data (metabolic cage). EchoMRITM body composition analyser (EchoMRI, Houstan, TX, USA) was used to measure lean and fat mass.
Data analysis	Flow cytometry data were analyzed using FlowJo v9.9.4. Statistics calculated using Prism version 7. ChIP and ATACseq track figures were generated using Integrated genome browser. RNAseq and ATACseq analysis softwares - featurecounts, Limma package. ChIPseq analysis software - Homer. CalR software was used to analyze metabolic cage data.

For manuscripts utilizing custom algorithms or software that are central to the research but not yet described in published literature, software must be made available to editors/reviewers. We strongly encourage code deposition in a community repository (e.g. GitHub). See the Nature Research guidelines for submitting code & software for further information.

Data

Policy information about availability of data

All manuscripts must include a data availability statement. This statement should provide the following information, where applicable:

- Accession codes, unique identifiers, or web links for publicly available datasets
- A list of figures that have associated raw data
- A description of any restrictions on data availability

Sequencing data generated for this study have been deposited in the Gene Expression Omnibus (GEO) database with accession number GSE121838.

Field-specific reporting

Please select the one below that is the best fit for your research. If you are not sure, read the appropriate sections before making your selection.

☒ Life sciences ☐ Behavioural & social sciences ☐ Ecological, evolutionary & environmental sciences

For a reference copy of the document with all sections, see nature.com/documents/nr-reporting-summary-flat.pdf

Life sciences study design

All studies must disclose on these points even when the disclosure is negative.

Sample size	Animal models used in this study are well established and yield low variance. Therefore, for each experiment, 3-5 animals were used and the experiment repeated with the same number of mice. Owing to low variance, statistical power was achieved with 3 mice the least.
Data exclusions	No data points were excluded
Replication	In vivo experiments were performed at least twice with minimum 3 mice per experiment. In vitro experiments were performed at least twice with 3 experimental replicates/ sample. All experimental replicates yielded comparable results. RNAseq and ATACseq - 2 replicates. Cells from 3 mice were pooled for each RNA and ATACseq sample.
Randomization	Not applicable. Age and sex matched mice of the same genetic background were used throughout.
Blinding	Blinding was not done. A fully informed data analysis was performed.

Reporting for specific materials, systems and methods

We require information from authors about some types of materials, experimental systems and methods used in many studies. Here, indicate whether each material, system or method listed is relevant to your study. If you are not sure if a list item applies to your research, read the appropriate section before selecting a response.

Materials & experimental systems

n/a	Involved in the study
☐	☒ Antibodies
☒	☐ Eukaryotic cell lines
☒	☐ Palaeontology
☐	☒ Animals and other organisms
☒	☐ Human research participants
☒	☐ Clinical data

Methods

n/a	Involved in the study
☒	☐ ChIP-seq
☐	☒ Flow cytometry
☒	☐ MRI-based neuroimaging

Antibodies

Antibodies used	Invitrogen/eBioscience – KLRG1 (2F1) FITC (Cat# 11-5893-82; Lot#1995313), BV711; Thy1.2 (30-H12) FITC (Cat#11-0903-85; Lot#4328351); gdTCR (ebioGL3) FITC (Cat#11-5711-82; Lot#E00635-1634); CD25 (PC61.5) PEcy7 (Cat#25-0251-82; 4323751); Gp38 (eBio8.1.1) PEcy7 (Cat#25-5381-82; Lot#1912145); KLRG1 (2F1) PEcy7 (Cat#25-5893-82; Lot#4300747); ST2 (RMST2-2) APC (Cat#17-9335-82; Lot#1952982); Tigit (GIGD7) eFluor660 (Cat#50-9501-82; Lot#E15694-104); GITR APC (Cat#17-5874-81; Lot#1983650); CD25 (PC61.5) APC (Cat#17-0251-82; Lot#4276862); TCRb (H57-597) PerCP Cy5.5 (Cat#45-5961-82; Lot#1927462); Foxp3 (FJK-16s) eFluor450 (Cat#48-577-82; Lot#1988692); Ly5.1 (A20) eFluor450 (Cat#48-0453-82; Lot#1993153); Gata3 (TWAJ) PE (Cat#12-9966-42; Lot#2010182), EOMES (Dan11mag) PerCPeFluor710 (Cat#46-4875-82; Lot#4288912). BD - Ly5.2 (104) FITC (Cat#561874; Lot#8281541); CD4 (GK1.5)BUV496 (Cat#612952; Lot#9098749); CD19 (1D3) BUV737 (Cat#564296; Lot#8039779); CD8a (53-6.7) BUV737 (Cat#564297; Lot#9030634); CD45.2 (104) BUV395 (Cat#564616;Lot#9176856); CD11b (M1/70) BUV737 (Cat#564443; Lot#8081887); KLRG1 (2F1) BV711 (Cat#564014; Lot#8339872),CD45.1 (A20) FITC (Cat#553775; Lot#6042599). BioLegend – F4/80 (BM8) FITC (Cat#123108; Lot#B257637); CD45.2 (104) BV605 (Cat#109841;Lot#B279618); CD4 (GK1.5) APC/cy7 (Cat#100414; Lot#B251980); CD11c (N418) BV711 (Cat#117349;Lot#B248202); CD69 (H1.2F3) BV711 (Cat#104537;Lot#B24311); F4/80 (BM8) BV605 (Cat#123133;Lot#B268952); CD140a (APA5) APC (Cat#135908; Lot#B257183); CD31 (BV421) (Cat#102423; Lot#B265878); CD73 (TY/11.8) PE (Cat#127206; Lot#B216418) R&D systems – mCCR2 A700 (Cat#FAB5538N; Lot#ADCV0317031). WEHI – NK1.1 (PK136) Alexa594.
Validation	All antibodies were validated by the suppliers.

Animals and other organisms

Policy information about studies involving animals; ARRIVE guidelines recommended for reporting animal research

Laboratory animals	Era−/−, Ar−/−, Arfl/fl, Ccr2-/-, Blimp1fl/fl, Blimp1GFP, Il33−/−, Il6−/−, Tnf−/−, Il1b−/− , Foxp3Cre, Foxp3RFP, IL10GFP, Rag-/-, Stat3fl/fl-creERT2, Cyp19-/- . All mice used were on C57BL/6J background except Il33-/- which is on C57BL/6N. Male and female mice were used for the study. Age of the mice ranged from 25-35 weeks. For hormone treatment (E-2 and T) experiments, 15 week old mice were used.
Wild animals	No wild animals were used in this project
Field-collected samples	None
Ethics oversight	Animal experiments were performed according to the animal ethics committee guidelines of Walter and Eliza hall Institute, Per MacCallum Cancer Centre and Peter Doherty institute for Infection and Immunity

Note that full information on the approval of the study protocol must also be provided in the manuscript.

Flow Cytometry

Plots

Confirm that:

☐ The axis labels state the marker and fluorochrome used (e.g. CD4-FITC).

☐ The axis scales are clearly visible. Include numbers along axes only for bottom left plot of group (a 'group' is an analysis of identical markers).

☐ All plots are contour plots with outliers or pseudocolor plots.

☒ A numerical value for number of cells or percentage (with statistics) is provided.

Methodology

Sample preparation	Cells isolated from lymphoid or non lymphoid tissues were surface stained with appropriate antibodies for 30 min at 4 degrees. Excess antibody was washed off and cells were analyzed. Sytox blue was used to identify dead cells. Dead cells were gated out during analysis. For intracellular staining, surface stained cells were fixed and permeabilized using eBioscience (Invitrogen) Foxp3 staining kit and appropriate antibody was added to detect transcription factors.
Instrument	Flow cytometry data was acquired using BD LSR Fortessa X20 (Diva software).
Software	Flow cytometry data was analyzed using FlowJo v9.9.4.
Cell population abundance	Cell populations analysed ranged from 500-10000 cells/ organ/mouse
Gating strategy	*Describe the gating strategy used for all relevant experiments, specifying the preliminary FSC/SSC gates of the starting cell population, indicating where boundaries between "positive" and "negative" staining cell populations are defined.*

☐ Tick this box to confirm that a figure exemplifying the gating strategy is provided in the Supplementary Information.